




Pedipalp anatomy of the Australian black rock scorpion, *Urodacus manicatus*, with implications for functional morphology

Russell D. C. Bicknell^{A,B,*} , Gregory D. Edgecombe^C, Christopher H. R. Goatley^{A,D,E}, Glen Charlton^F and John R. Paterson^A

For full list of author affiliations and declarations see end of paper

*Correspondence to:

Russell D. C. Bicknell
Palaeoscience Research Centre, School of
Environmental & Rural Science, University of
New England, Armidale, NSW 2351, Australia
Email: rdcbicknell@gmail.com,
rbicknell@amnh.org

Handling Editor:

Paul Cooper

ABSTRACT

Pedipalps – chelate ‘pincers’ as the second pair of prosomal appendages – are a striking feature of scorpions and are employed in varied biological functions. Despite the distinctive morphology and ecological importance of these appendages, their anatomy remains underexplored. To rectify this, we examined the pedipalps of the Australian black rock scorpion, *Urodacus manicatus*, using a multifaceted approach consisting of microcomputed tomography, scanning electron microscopy, energy dispersive X-ray spectroscopy, and live pinch force measurements. In doing so, we document the following aspects of the pedipalps: (1) the musculature in three dimensions; (2) the cuticular microstructure, focusing on the chelae (tibial and tarsal podomeres); (3) the elemental construction of the chelae teeth; and (4) the chelae pinch force. We recognise 25 muscle groups in *U. manicatus* pedipalps, substantially more than previously documented in scorpions. The cuticular microstructure – endo-, meso-, and exocuticle – of *U. manicatus* pedipalps is shown to be similar to other scorpions and that mesocuticle reinforces the chelae for predation and burrowing. Elemental mapping of the chelae teeth highlights enrichment in calcium, chlorine, nickel, phosphorus, potassium, sodium, vanadium, and zinc, with a marked lack of carbon. These elements reinforce the teeth, increasing robustness to better enable prey capture and incapacitation. Finally, the pinch force data demonstrate that *U. manicatus* can exert high pinch forces (4.1 N), further highlighting the application of chelae in subduing prey, as opposed to holding prey for envenomation. We demonstrate that *U. manicatus* has an array of adaptations for functioning as a sit-and-wait predator that primarily uses highly reinforced chelae to process prey.

Keywords: Australia, energy dispersive X-ray spectroscopy, micro-computed tomography, microstructure, morphology, musculature, scanning electron microscopy, scorpions, *Urodacus manicatus*.

Received: 26 October 2023

Accepted: 5 April 2024

Published: 13 May 2024

Cite this: Bicknell RDC *et al.* (2024)

Pedipalp anatomy of the Australian black rock scorpion, *Urodacus manicatus*, with implications for functional morphology. *Australian Journal of Zoology* **72**, ZO23044. doi:10.1071/ZO23044

© 2024 The Author(s) (or their employer(s)). Published by CSIRO Publishing.

This is an open access article distributed under the Creative Commons Attribution 4.0 International License (CC BY).

OPEN ACCESS

Introduction

Chelate pedipalps are one of the most striking structures displayed by scorpions. These modified prosomal appendages serve disparate functions, including predation (Lamoral 1971; Simone and van der Meijden 2018; Leeming 2019; Cunha *et al.* 2022), defence (van der Meijden *et al.* 2013), and burrowing (Harrington 1977; Abdel-Nabi *et al.* 2004). As such, the mechanics (van der Meijden *et al.* 2012a; Bicknell *et al.* 2022), structure (Zhao *et al.* 2016; Zhang *et al.* 2023), and general biology (Snodgrass 1952) of pedipalps have been discussed at length.

The pedipalp chelae are one of few regions of the scorpion body to have been subjected to three dimensional (3D) documentation (van der Meijden *et al.* 2012a; Simone and van der Meijden 2018; Kellersztein *et al.* 2019). This information is supplemented by 3D data for the stinger (Zhao *et al.* 2016; van der Meijden and Kleinteich 2017; Simone and van der Meijden 2021), metasomal muscles (Günther *et al.* 2021a, 2021b), and the vascular system (Wirkner and Prendini 2007). Limited examination of scorpion appendages using

3D methods contrasts with the current state of research into other arachnids, such as camel spiders (van der Meijden *et al.* 2012b; Runge and Wirkner 2020), pseudoscorpions (Michalski *et al.* 2022), whip scorpions (Grams *et al.* 2018), and whip spiders (Schmidt *et al.* 2022). However, scorpion appendage musculature has a long history of documentation in two dimensions (2D) (Lankester 1885; Snodgrass 1948; Alexander 1967; Durale and Vyas 1968; Manton 1977; Bowerman and Root 1978; Shultz 1989, 1992, 2007; Wolf and Harzsch 2002), providing a precedent for presenting such data within a more interactive and tangible framework.

Other aspects of the pedipalps that require further study are the microstructure and chemical composition of the cuticle. Scorpion diversity has inspired extensive documentation of many exoskeletal structures, and, as a result, the group has the most comprehensive information on cuticle among chelicerates (Krishnan 1953; Kennaugh 1959; Malek 1964; Mutvei 1978; Filshie and Hadley 1979; Dalingwater 1987; Kellersztein *et al.* 2019, 2021). However, the pedipalps, particularly the chelate sections, have not been subject to detailed study (see Mutvei 1978; Kellersztein *et al.* 2019, 2021), and there are limited data on the chemical composition of chelae (Schofield *et al.* 2003).

To better understand the morphofunctionality of the pedipalps as a key adaptation of scorpions, we present an integrative, multifaceted investigation of an exemplar species framed around four core scientific questions:

- (1) How is the morphology of scorpion pedipalp musculature expressed, how many muscles can be identified, and to what extent can we homologue these muscles with other scorpion species?
- (2) What is the cuticular microstructure of pedipalps and does microstructure vary in different regions and cross-sectional orientations?
- (3) What are the elemental constituents of scorpion pedipalp appendages and how can the elemental composition be used to inform functional interpretations?
- (4) How much force can scorpion pedipalps exert while pinching and what does this mean for species ecology?

Beyond these scientific questions, we aim to illustrate how a synthesis of methodologies can build impactful frameworks to thoroughly document arthropod predatory morphologies. Using this objective, we highlight how multiple topics in animal ecology and morphology can be explored.

To address these questions, we examine a well-known Australian scorpion species, *Urodacus manicatus* (Thorell 1876) (Fig. 1), as a case study. This species was chosen because its distribution (Pocock 1888; Southcott 1955; Koch 1978; Harvey and Volschenk 2002), ecology (Southcott 1955; Smith 1966; Shorthouse and Marples 1982; Warburg and Rosenberg 1994; Holden 1997; Woodman 2008), toxicology (Lowe and Farrell 2011; Luna-Ramirez *et al.* 2017),

taxonomy (Pocock 1898; Harvey and Volschenk 2002; Soleglad *et al.* 2005), and phylogenetic position (Soleglad *et al.* 2005) are well documented. In addressing our four core research questions, we present a 3D anatomical atlas of the pedipalp muscles, and document the cuticular microstructure, elemental composition, and pinch force of the chelae of *U. manicatus*.

Materials and methods

Specimen collection

Five individuals of *Urodacus manicatus* were collected from a private property in Invergowrie, New South Wales, Australia (coordinates: 30°31'29"S, 151°30'20"E). Individuals were sampled at night, located using an ultraviolet (UV) light source during the Australian summer of February 2020. Based on the enlarged mesosoma, relatively small pectines, and lack of genital papillae, the specimens are identified as females; *U. manicatus* does not exhibit notable pedipalp sexual dimorphism. Two complete specimens, in addition to three pedipalps extracted post-mortem from two individuals are housed in the arthropod collection of the Natural History Museum (NENH-AR) at the University of New England (UNE), Armidale, Australia; specimen numbers are NENH-AR-00015, NEHM-AR-00016, NENH-AR-00017, NEHM-AR-00018, and NENH-AR-00019. The two largest specimens (NENH-AR-00015, NEHM-AR-00016) were initially kept alive in captivity, fed crickets, and used to determine pinch force values. The other two individuals from which pedipalps were removed (represented by NENH-AR-00017, NEHM-AR-00018, NENH-AR-00019) were frozen soon after collection, while NEHM-AR-00015 and NEHM-AR-00016 were frozen after pinch force data were gathered. The largest individual (NEHM-AR-00015) was selected for microcomputed tomography (micro-CT) scanning and reconstruction. The fifth (unregistered) specimen was released after being photographed under sunlight and UV light using a Canon PowerShot SX60 HS camera.

Micro-CT scanning and 3D reconstruction

Specimen NEHM-AR-00015 was micro-CT scanned to document the pedipalp muscles. Prior to scanning, it was submerged in ethanol to dehydrate muscles for more effective identification in the micro-CT scan. A scan with just dehydration through ethanol was conducted. Contrast-enhancement using phosphotungstic acid (PTA) (Metscher 2009; Gignac *et al.* 2016) was subsequently undertaken with NEHM-AR-00015. In this case, the specimen was immersed in a 70 mL mixture of 70% ethanol and PTA, with a PTA concentration of 0.5%. To examine possible increase in density difference due to the PTA, scans were conducted 12, 36, 48, 72, 168, and 192 hours after submergence.

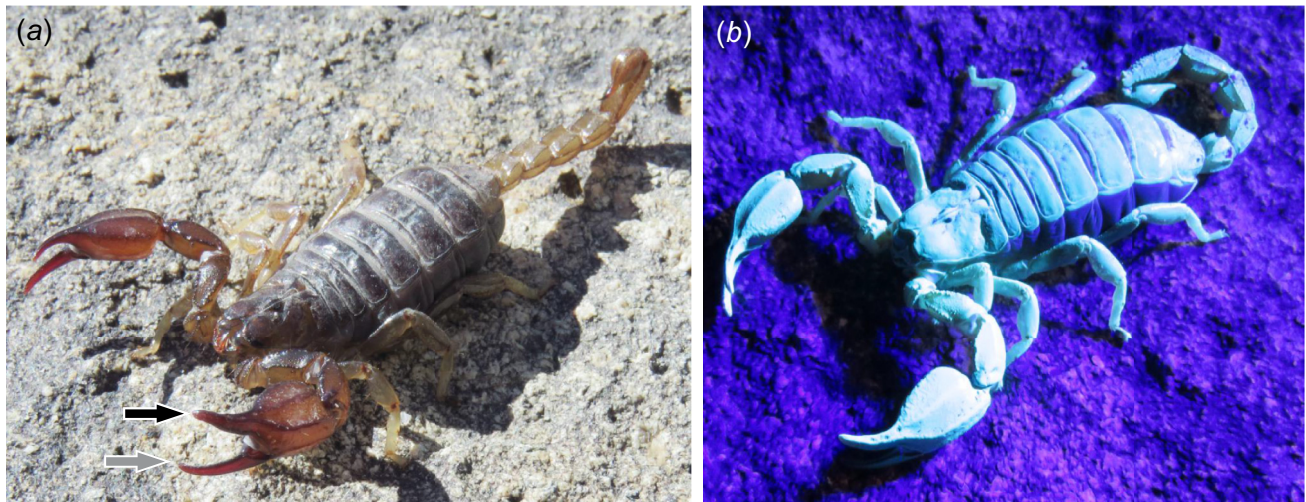


Fig. 1. The black rock scorpion *Urodacus manicatus*. (a) Individual in sunlight. Black arrow indicates fixed finger (tibia) and grey arrow indicates moveable finger (tarsus) of the pedipalps. (b) The same individual under UV light at night.

However, these scans were abandoned as they generated lower contrast images compared to ethanol fixation. While this might reflect slow diffusion of the PTA through the specimen, we did not pursue this approach further as the scan of the ethanol-only condition was sufficient. NEHM-AR-00015 was scanned in a GE-Phoenix v|tome|x micro-CT scanner using the 'Direct' tube at UNE, under optimised X-ray tube settings (200 kV, 100 A, 1000 × 1000 pixels capture conditions, an isotropic voxel side length of 22.5 µm, and a rotation step of 0.1125°). The scan focused on the pedipalp and prosoma. Scan data were captured and reconstructed using *datos|x* software ver. 2.2.1 (phoenix, Wunstorf, Germany).

The scan was imported into *Mimics* ver. 23.0 (Materialise, Leuven, Belgium) and segmented using the 'Segmenting' tool. The prosoma, anterior walking legs, pedipalp podomeres, and pedipalp muscles were segmented using the 'Segmenting' tool (Supplemental Fig. 1). Muscle descriptions presented here are based on the scans, muscle fibre directions in scans, 3D reconstructions, and publications previously detailing scorpion pedipalp muscles (Vyas 1970; Shultz 2007). To identify a muscle as an independent unit, two criteria were considered. Firstly, segmented muscles were reconstructed in 3D in *Mimics* and correspondences to muscles in published examples were identified (Vyas 1970; Shultz 2007). Secondly, other muscle groups were defined by matching morphologies and common attachment points, muscle bands and fibre orientation, and positions in both pedipalps. In taking this approach, we consider the identified muscles to be functionally and morphologically independent. Muscles were described following the terminology in Shultz (2007). This includes the origin location, insertion location, and the morphology of the muscles themselves. Muscles are numbered proximal to distal along the appendage. Once the digital dissection was complete, 3D models of the exoskeleton and individual muscles were exported as .STL files from *Mimics*

and imported into *Geomagic Studio* (3D Systems, North Carolina, USA). All reconstructions were smoothed in *Geomagic Studio*. Smoothed .STL files were exported from *Geomagic Studio*, and a 3D PDF was generated using *Tetra4D*. Distinct muscles were grouped together and distinctly coloured to delineate the different muscle groups. Supplemental Fig. 1 is available from the following link: [10.17605/OSF.IO/GD7TV](https://doi.org/10.17605/OSF.IO/GD7TV). All scan data are available as unedited .TIFF stacks on MorphoSource.org at [ark:/87602/m4/495251](https://doi.org/10.26434/chemrxiv-2023-04).

Cuticle microstructure and elemental mapping

The three extracted pedipalps were embedded in epoxy blocks for sectioning in transverse, sagittal, and coronal planes. Embedded appendages were ground through to section the pedipalps. Sectioned surfaces were polished, gold coated and imaged using the JEOL JSM-6010LA Scanning Electron Microscope (SEM) at UNE. Accelerating voltages of 10 kV (NEHM-AR-00019) and 20 kV (NEHM-AR-00017, NEHM-AR-00018) were used to acquire the secondary electron (SE) images of the appendages.

The elemental composition of the chelae teeth and proximal cuticle for NEHM-AR-00018 and NEHM-AR-00019 were derived with SEM Energy Dispersive X-Ray Spectroscopy (EDS). The specimens were gold coated and analysed under 20 kV for 6 h in the JEOL JSM-6010LA SEM to produce a series of elemental maps. Coating arthropod cuticle with inert metals follows previously developed methodologies (Tadayon *et al.* 2020; Bentov *et al.* 2021). This approach avoids build-up of charge while specimens are in the SEM. We did not carbon coat the specimens as this would have rendered carbon measurements unreliable. No distinction regarding elemental distributions in EDS has been reported when different coating materials have been used (Bentov *et al.* 2021). As such, we are confident our approach did not

impact the distribution and relative abundance of elements within the examined sections. Additionally, backscatter images of mapped regions were made under these conditions. Preliminary maps were made to reveal the most informative elements for mapping. Elements, such as iron, were therefore not included as they showed no notable abundance in the preliminary maps.

Chelae force measurements

To measure the pinch force, a force-sensitive resistor (FlexiForce A101 Sensor; Tekscan Inc., Massachusetts, United

States) was constructed using a voltage divider circuit (Fig. 2a). The A101 sensor was used as its small size (3.8 mm diameter; Fig. 2d) was the most appropriate for measuring pinch force of *U. manicatus* pedipalps, and helped to avoid unequal loading during pinching. A 50 Hz frequency was used with an analogue input pin and an Adafruit Feather ATSAMD21 Cortex M0 Adafruit (Adafruit Industries, New York, United States) prototyping board. This approach to building a force transducer had not previously been conducted and was novel for this project (Fig. 2c). Sensor calibrations were needed to calculate pinch force. These calibrations were derived by

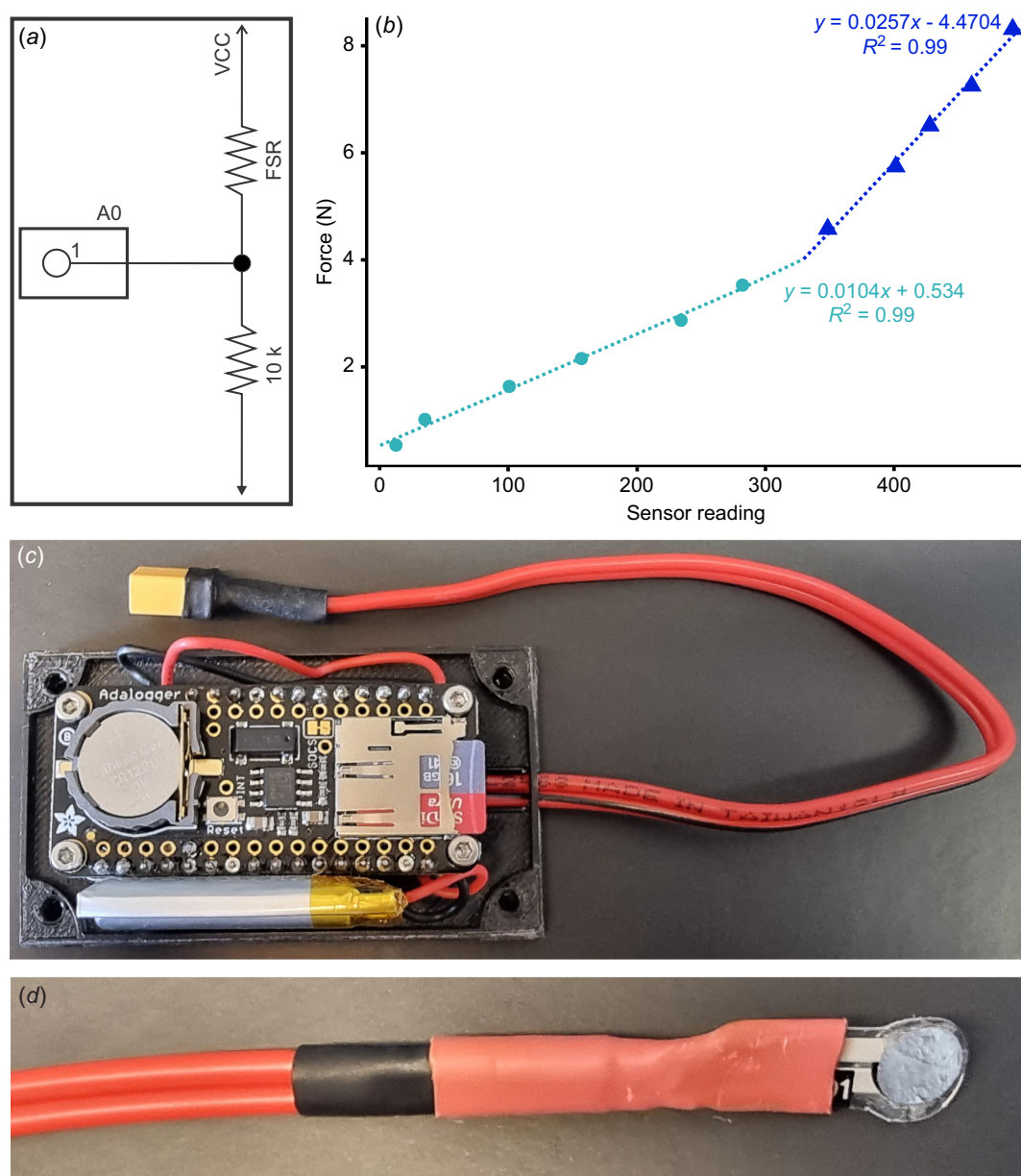


Fig. 2. Details of force transducer for pedipalp pinch force tests. (a) Schematic of the circuit used for the transducer. (b) Calibration data used to derive equations for determining force output from the transducer. (c) An image of the force transducer. (d) Example of force plate used. Abbreviations: A0, Analogue measuring point; FSR, Force sensitive resistor; N, Newtons; VCC, Power source (5 V); 10k, Voltage dividing resistor.

adding weight to the sensor, increasing the force registered through gravity. Two linear equations representing the logarithmic relationship between resistance and force were derived using Microsoft Excel and used to calculate force based on the measured values, while allowing the closest fit of data to calibration values (Fig. 2b; Supplemental Data 1). This approach allowed force data to be gathered at a frequency of 1000 Hz. However, to limit the dataset to a manageable number of observations (<1000), we gathered data at a frequency of 50–100 Hz. To derive pinch force values, NENH-AR-00015 and NEHM-AR-00016 were agitated and prompted to pinch down on the resistor. The outer edge of the force transducer was positioned within the pincer, close to the moveable and fixed finger articulation to induce pinching and avoid unequal loading. This experiment was conducted between 20 and 25°C. This resulted in a dataset of 836 distinct force data points from seven distinct pinch events (NEHM-AR-00015) and 788 distinct force data points from four distinct pinch events (NENH-AR-00016). Data were plotted as histograms to examine pinch force distribution.

Results

Pedipalp musculature

The anteriormost walking legs, fixed and movable chelical segments, labrum, prosoma, and pedipalp podomeres (coxa, trochanter, femur, patella, tibia, and tarsus) were resolved (Fig. 3). The pedipalp morphology consists of reduced, stout coxae and trochanters, elongated femurs and patellae, bulbus manus regions in the tibia, with elongate and robust tibial and tarsal fingers. In total, 25 muscle groups associated with the pedipalps were identified (Table 1; Figs 4, 5, 6, 7 and 8), expanding on the muscles presented by Vyas (1970) and Shultz (2007) (Table 1). These additional muscles are primarily located within the trochanter (Muscles 8–13) and are generally smaller and located proximally to larger muscle groups, so may have been missed or grouped together in previous studies (Table 1). The 25 muscles include groups with a prosomal origin (Muscles 1–5; see depiction of Muscles P1, P2, P3, P8, P9 in Shultz 2007; Table 1) and groups located wholly within the pedipalps (Muscles 6–25). Most pedipalp muscles have an origin proximally within their respective appendage segments (Figs 4, 5, 6, 7 and 8) and insert within or proximal to the next distal podomere (Table 1). There are two muscles with large tendons that extend to more distal podomeres: Muscles 9 and 24. In the micro-CT scan, several longer muscle groups show breakage or truncation. In particular, we note that Muscles 1, 2, and 21 and the tendons of Muscles 9 and 24 show this condition. These breakages reflect fixing from ethanol and muscle damage during dehydration.

Pedipalp microstructure

Under the SEM, cuticle structures (*sensu* Richards 1951; Dalingwater 1987) were observed along the sectioned appendages (Fig. 9). In the sagittal section (NENH-AR-00017), laminate endocuticle is ~70 µm thick, with single lamina ~5 µm thick, and exocuticle 8 µm thick (Fig. 9d). There is a notable lack of laminae in the tibial fixed finger, but 14–60 µm wide pore canals are observed here (Fig. 9b).

Cuticle morphology along both fingers is visible in the coronal section (Fig. 10a; NENH-AR-00018). Laminate endocuticle (~80–200 µm, single lamina ~5 µm thick) is overlain by 70–130 µm-thick mesocuticle (*sensu* Zhang *et al.* 2023) that lacks any structure when viewed coronally. Above the mesocuticle is thin exocuticle (12–17 µm) with 2–5 laminae (~4 µm thick) (Fig. 10a). Pore canals up to 180 µm wide are present in the finger and proximal tarsal regions. Finger teeth are darker than other cuticular areas in backscatter imagery and show tooth roots extending into the fingers (Fig. 10b).

In the transverse section (Fig. 11; NENH-AR-00019), the laminate endocuticle is ~90 µm thick, with single lamina ~5 µm thick. Regions where the endocuticle extends to the teeth are observed, with a thickness of ~290 µm (Fig. 11a). Where the endocuticle does not extend to the teeth, the endocuticle is overlain by mesocuticle, consisting of vertically stacked cuticle that is 60–70 µm thick. The mesocuticle is overlain by exocuticle that is 20–30 µm thick, with ~4 µm thick laminae. Pore canals reaching 165 µm in length and cross-cut endo-, meso-, and exocuticle layers. Teeth are lighter than other cuticle in backscatter imagery (Fig. 11b).

Elemental construction of chelae cuticle and teeth

Elemental maps of the coronal and transverse sections focusing on the teeth show similar elemental distributions (Figs 10, 11; NENH-AR-00018, NENH-AR-00019). There is a pervasive enrichment of chlorine (Cl), nickel (Ni), phosphorus (P), potassium (K), sodium (Na), vanadium (V), zinc (Zn), and oxygen (O) in the teeth and roots (Figs 10, 11) and a notable lack of carbon (C) in the teeth. Calcium (Ca) has limited enrichment along the chelae edges and teeth roots. Magnesium (Mg) has a consistent distribution across teeth and cuticle. The general pedipalp cuticle is distinctly lacking in Na, Zn, V, and Ni, has a limited abundance of Cl, P, K, Ca, and O, and an enrichment of C relative to teeth.

Pedipalp pinch force

Pinch force values from specimens NENH-AR-00015 ($n = 836$ measurements) and NENH-AR-00016 ($n = 788$ measurements) have similar distributions. Both distributions are right skewed, with major peaks at about 1 N (Fig. 12). NENH-AR-00016 has two smaller peaks at 2.8 N and 4.2 N, and a mean pinch force of 1.84 N. NENH-AR-00015 has three smaller peaks at 2.0 N, 3.2 N, and 4.2 N, and a mean

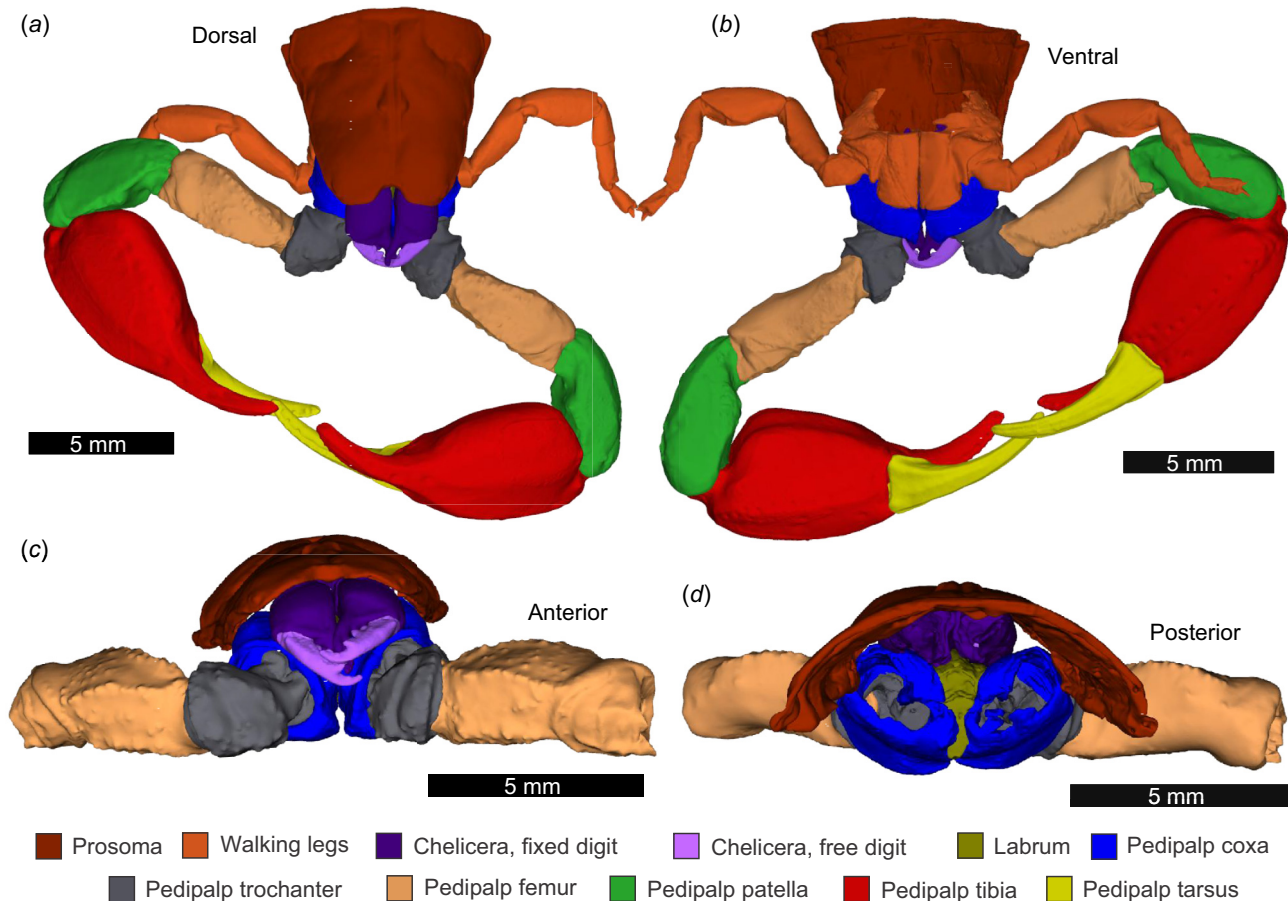


Fig. 3. 3D reconstructions of the anterior region of *Urodacus manicatus*, as modelled by micro-CT scanning. NEHM-AR-00015. (a) Dorsal view. (b) Ventral view. (c) Anterior view excluding patella, tibia, and tarsus. (d) Posterior view excluding patella, tibia, and tarsus. The 3D PDF is found in Supplemental Fig. 1.

pinch force of 2.22 N. NENH-AR-00015, the larger of the two studied individuals, tended to produce higher pinch forces.

Discussion

Using micro-CT to inform on scorpion anatomy

Our documentation of pedipalp muscles expands on previous research by Vyas (1970, on *Heterometrus fulvipes*) and Shultz (2007, on *Heterometrus spinifer*) by presenting 20 muscle groups located solely within pedipalp podomeres and five muscle groups with prosomal origins. Based on the origin, insertion, and muscle shape, we can suggest homologies between 18 of these muscles across these studies (Vyas 1970; Shultz 2007). This demonstrates that at least seven muscles documented herein are novel. These data illustrate how pedipalp muscles engage distinct podomeres. For example, the long tendon of Muscle 9 illustrates that pedipalp coxal muscles engage more distal pedipalp regions than previously realised. These muscle reconstructions have the potential to support arguments about possible homologies between

the pedipalp and walking leg muscles of scorpions (see Shultz 2007 for a detailed discussion). In comparing muscles reconstructed here with previous depictions of walking leg muscles (Snodgrass 1952; Shultz 1989; Wolf and Harzsch 2002), similarities in muscle arrangements in the femur and patella can be drawn. In particular, we propose that pedipalp Muscles 17 and 18 of *Urodacus manicatus* (Fig. 7) are homologous with leg Muscles 19 and 16, respectively, of *Pandinus* sp. illustrated by Snodgrass (1952, fig. 19G), and Muscles 22 and 23 (Fig. 7) correspond to Muscles 21 and 20 (cf. Snodgrass 1952, fig. 19G). A detailed examination of these muscles using similar tools is needed to document these proposed homologies more thoroughly and confidently.

Functional interpretations for musculature can be drawn using muscle origins, insertions, and size. Muscles 1–5 have prosomal origins, inserting into the coxae. As they are extrinsic muscles (Beck 1885; Lankester 1885; Shultz 2007), they reinforce and maintain the coxal position. Muscles 6–8 and 10–13 are positioned within the coxae, with insertion into the trochanter, likely permitting the large range of motion for the articulation, similar to muscles in the walking legs

Table 1. Summary of morphologies, orientations, origins, and insertions of muscles documented here in NENH-AR-00015.

Muscle number	Origin	Insertion	Muscle morphology	Muscle name in Vyas (1970) using <i>Heterometrus fulvipes</i> (Koch 1837)	Muscle name in Shultz (2007) using <i>Heterometrus spinifer</i> (Ehrenberg, 1828)	Figure
Muscle 1	Medial, ventral cuticle prosoma	Distolateral coxa	Large, elongate, tapering to insertion	? Muscle depressor trochanteris posterioris	Pedipalp 9	Fig. 5
Muscle 2	Mediolateral, ventral cuticle prosoma	Proximolateral margin coxa	Elongate, limited tapering to insertion	–	Pedipalp 8	Fig. 5
Muscle 3	Anterolateral, ventral cuticle prosoma	Proximodorsal margin coxa	Slender, tapering to insertion	Muscle abductor coxalis	Pedipalp 2	Fig. 5
Muscle 4	Mediolateral, ventral cuticle prosoma, more lateral than Muscle 3	Proximoventral margin coxa	Elongate, marked tapering to insertion	Muscle protractor coxalis	Pedipalp 3	Fig. 5
Muscle 5	Anterolateral, ventral cuticle prosoma	Distolateral coxa	Elongate, limited tapering to insertion	? Muscle promotor coxalis	Pedipalp 1	Fig. 5
Muscle 6	Proximomedial coxa	Proximolateral margin trochanter	Large, no tapering to insertion	Muscle levator trochanteris obliquus	–	Fig. 6
Muscle 7	Proximoventral coxa	Proximomedial margin trochanter	Large, ovate, no tapering to insertion	?Muscle depressor trochanteris anterioris	–	Fig. 6
Muscle 8	Proximolateral to proximoventral coxa	Proximolateral margin trochanter	Large, reniform, limited tapering to insertion	?Muscle levator trochanteris ventralis	–	Fig. 6
Muscle 9*	Proximolateral to proximoventral coxa, nested within Muscle 8	Tendon extending to proximomedial patella	Round, extending into elongate tendon	–	–	Figs 6 and 7
Muscle 10*	Proximomedial coxa, nested within Muscle 7	Proximoventral margin trochanter	Elongate, limited tapering to insertion	–	–	Fig. 6
Muscle 11*	Proximoventral through to ventromedial coxa	Lateral, proximoventral margin trochanter	Fan shape, increasing in size towards insertion	–	–	Fig. 6
Muscle 12*	Lateral, distoventral coxa	Medial, proximoventral margin trochanter	Subrectangular, limited tapering	–	–	Fig. 6
Muscle 13*	Distomedial coxa	Medial, proximoventral margin trochanter	Triangular	–	–	Fig. 6
Muscle 14*	Proximomedial though to ventral region trochanter	Medial, proximoventral margin femur	Round, tapering into elongate shape towards insertion	–	–	Fig. 7
Muscle 15	Dorsomedial trochanter	Dorsodistal trochanter and proximodorsal margin femur	Fan shaped, tapering to insertion	? Muscle levator femoralis	–	Fig. 7
Muscle 16	Dorsodistal trochanter	Proximoventral femur	Fan shaped, tapering to insertion	? Muscle depressor femoralis posterioris	–	Fig. 7

(Continued on next page)

Table 1. (Continued).

Muscle number	Origin	Insertion	Muscle morphology	Muscle name in Vyas (1970) using <i>Heterometrus fulvipes</i> (Koch 1837)	Muscle name in Shultz (2007) using <i>Heterometrus spinifer</i> (Ehrenberg, 1828)	Figure
Muscle 17	Distal trochanter	Ventral femur, half way along femur	Elongate, marked tapering to insertion	? Muscle depressor femoralis anterioris	–	Fig. 7
Muscle 18	Proximo-dorsolateral to disto-dorsolateral femur	Proximodorsal margin patella	Large, fan shaped, tapering to insertion	Muscle depressor patellae anterioris, Muscle depressor patellae posterioris	–	Fig. 7
Muscle 19	Proximo-ventrolateral femur	Proximoventral margin patella	Fan shaped, tapering to insertion	Muscle depressor patallae ventralis	–	Fig. 7
Muscle 20	Proximomedial at trochanter-femur articulation	Proximomedial margin patella	Elongate, no tapering	Muscle depressor patellae internus	–	Fig. 7
Muscle 21*	Proximo-ventrolateral femur	Proximomedial margin patella	Elongate, no tapering		–	Fig. 7
Muscle 22	Proximo-ventrolateral and proximo-ventromedial patella	Proximolateral margin tibia	Fan shaped, two major sections, tapering to insertion	Muscle extensor tibialis	–	Fig. 8
Muscle 23	Proximo-dorsolateral and proximo-dorsomedial patella	Proximomedial margin tibia	Fan shaped, two major sections, tapering to insertion	Muscle flexor tibialis	–	Fig. 8
Muscle 24	Distoventral patella	Tendon extending to tarsus	Fan shaped tapering rapidly into elongate tendon passing through Muscle 25	Muscle depressor taraslis posterioris	–	Fig. 8
Muscle 25	All surfaces of tibia	Proximal tarsus	Large, ovate to fan shaped	Muscle depressor taraslis anterioris	–	Fig. 8

Proposed homologies with the pedipalp muscles in Vyas (1970) and Shultz (2007) are included. '*' indicates new muscles identified here. '–' indicates that this muscle was not examined in the comparative publications. '?' indicates an uncertain homology based on comparing our reconstructions with other publications. See Figs 5–8 and Supplemental Fig. 1.

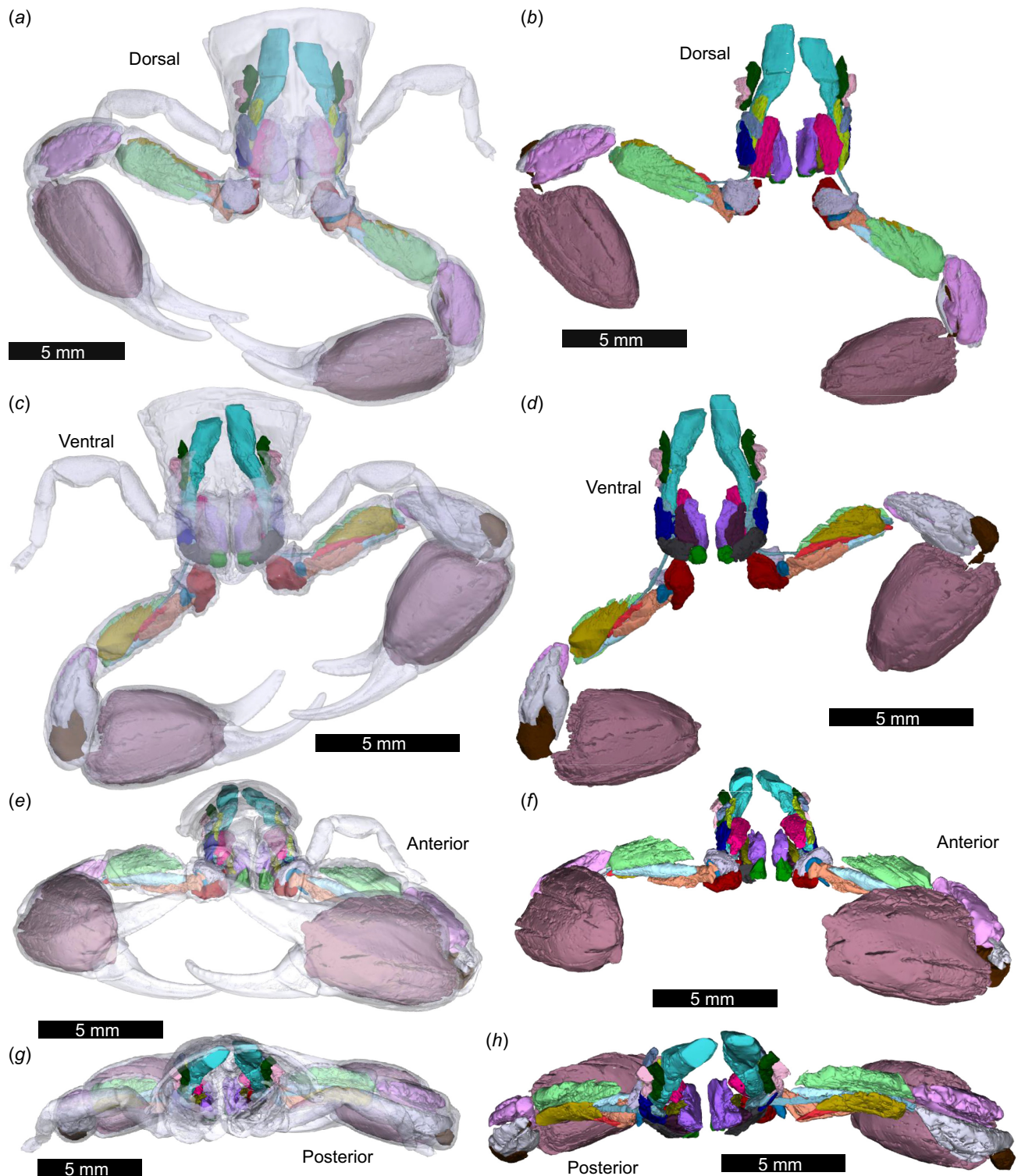


Fig. 4. 3D reconstructions of all identified prosomal and pedipalp muscles in NEHM-AR-00015, as modelled from micro-CT scanning. No key is included as some groups are not easily visualised when all muscles are illustrated. Separate muscles are illustrated in Figs 5–8. (a, c, e, g) Muscles with the exoskeleton as transparent. (b, d, f, h) Muscles without the exoskeleton. (a, b) Dorsal view. (c, d) Ventral view. (e, f) Anterior view. (g, h) Posterior view. All muscles are coloured separately. The 3D PDF associated with this reconstruction is found in Supplemental Fig. 1.

(Snodgrass 1952). Muscle 9, extending from the coxa to the patella as a tendon, may function to rapidly retract the

more distal pedipalp podomeres, possibly during or after capturing prey. This muscle apparently does not have an

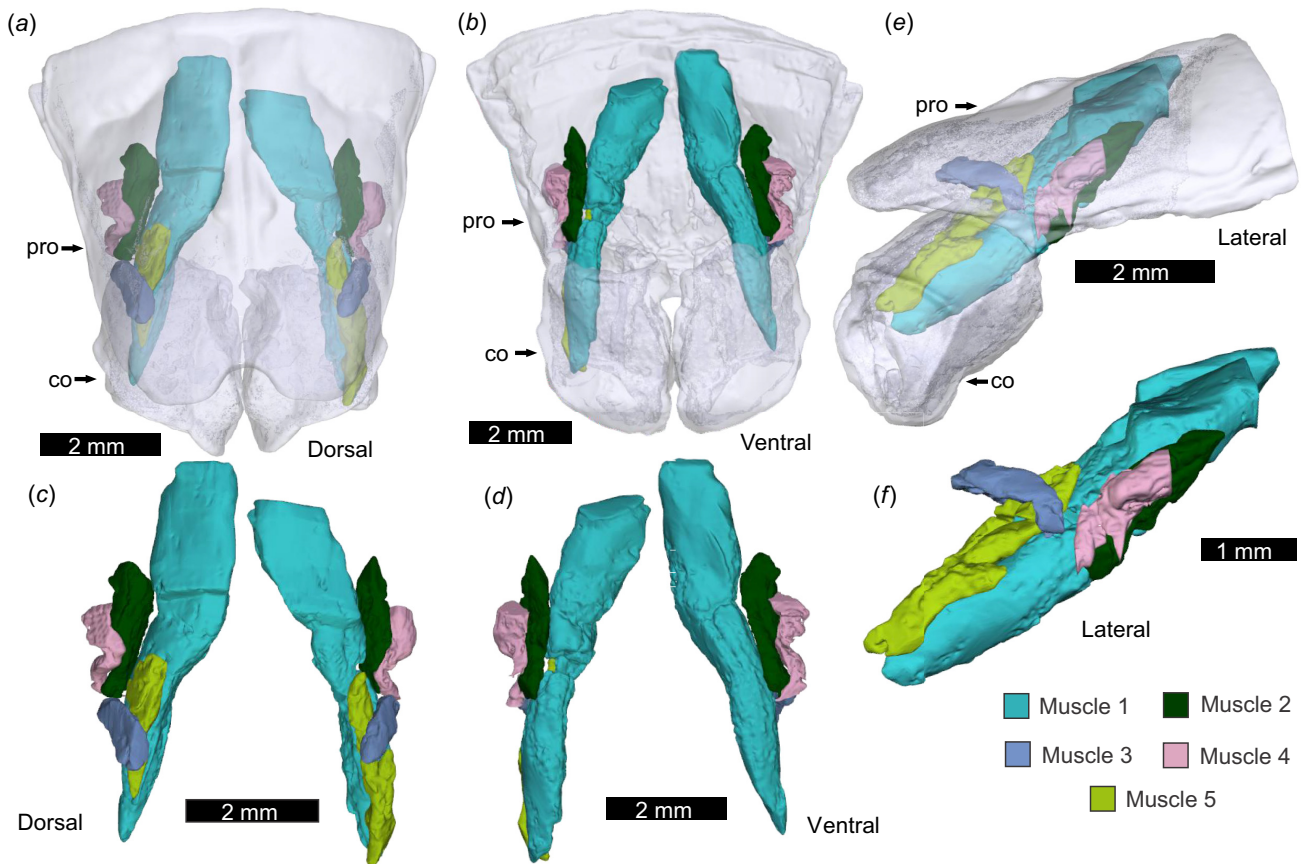


Fig. 5. Pedipalp muscles with prosomal origins, as modelled by micro-CT scanning. NEHM-AR-00015. (a, b, e) Prosoma and coxa as transparent. (c, d, f) Muscles without the exoskeleton. (a, c) Dorsal view. (b, d) Ventral view. (e, f) Left lateral view. Abbreviations: co, coxa; pro, prosoma. The 3D PDF associated with this reconstruction is found in Supplemental Fig. 1.

immediate analogue for comparison within other scorpion appendages. However, Muscle 9 is morphologically comparable to Muscle 10 of horseshoe crab walking legs (Snodgrass 1952, fig. 11a; Bicknell *et al.* 2018a, fig. 6) which is a flexor that moves the patella and other distal podomeres of the xiphosurid appendage towards more proximal podomeres and the body (Shultz 1989; 2001). A similar tendon extends across multiple appendage podomeres in the scorpion pedipalp. This morphological similarity suggests a comparable function – as a flexor muscle that moves the appendage towards the body, after attacking, or in defence. Such an explanation is also possible for Muscle 21 that could be used to retract the patella. Muscles 14–16 inserting proximal to the patella from the femur also permit a large range of motion for the patella–femur articulation. Muscles 17–20 are likely used to rotate and position the pedipalps relative to the prosoma. Developing on the homology with the walking leg muscles documented by Snodgrass (1952), Muscles 22 and 23 are flexor and extensor muscles, respectively. Among other possible uses, such as mating (Kellersztein *et al.* 2019), the large size of these muscles can be used to pull prey to the mouth for processing. Finally, Muscles 24 and 25 are well

documented in other taxa as the muscles used in the closing and opening of the tarsal podomere (Snodgrass 1952; van der Meijden *et al.* 2012a; Simone and van der Meijden 2021). More confident determination of the muscle roles discussed here requires *in vitro* examination of muscle movement (see Walker *et al.* 2014).

Identifying and reconstructing muscle clusters in 3D represents an important approach for testing hypotheses on the synapomorphies in related groups. One possible direction for this application of 3D anatomy is the grouping of scorpions and pseudoscorpions into Panscorpiones based on phylogenomics and rare genomic changes (Ontano *et al.* 2021); the traditional sister group hypothesis between pseudoscorpions and solifuges is challenged by the latter not sharing a whole genome duplication characteristic of arachnoplumonate arachnids (Gainett *et al.* 2024). In this case, one could determine whether the muscles groups in scorpion pedipalps are also observed in pseudoscorpion taxa. While pseudoscorpion coxal muscles have been documented in 3D (Michalski *et al.* 2022), a detailed consideration of muscles in their pedipalps has not yet been undertaken in a 3D context.

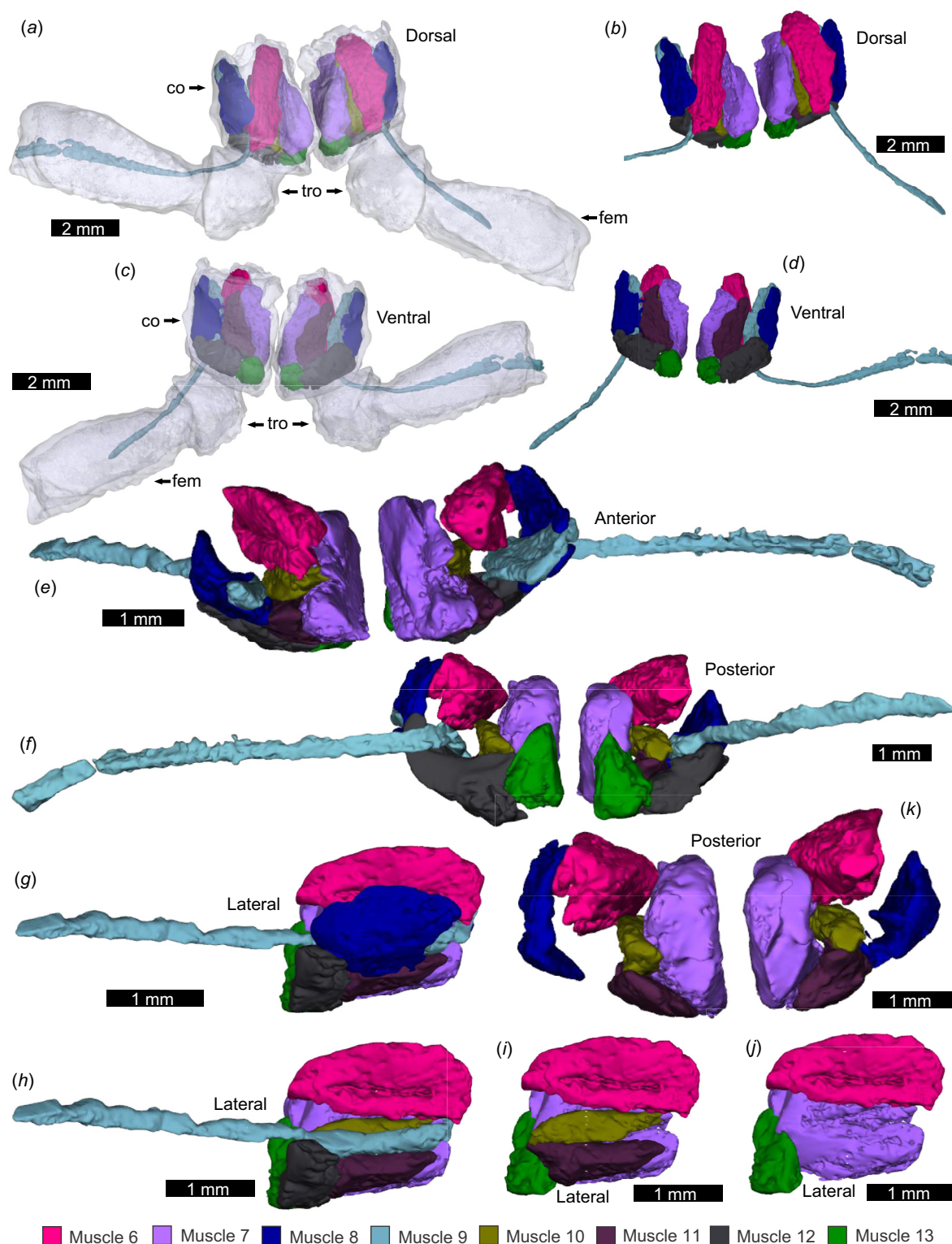


Fig. 6. Pedipalp muscles with coxal origins, as modelled from micro-CT scanning. NEHM-AR-00015. (a, c) Coxa, trochanter, and femur transparent with muscles. (b, d–j) Muscles without the exoskeleton. (a, b) Dorsal view. (c, d) Ventral view. (e) Anterior view. (f) Posterior view. (g–j) Left lateral view showing digital dissection of superimposed muscles. (k) Posterior view owing digital dissection of superimposed muscles. Abbreviations: co: coxa; fem: femur; tro: trochanter. The 3D PDF associated with this reconstruction is found in Supplemental Fig. 1.

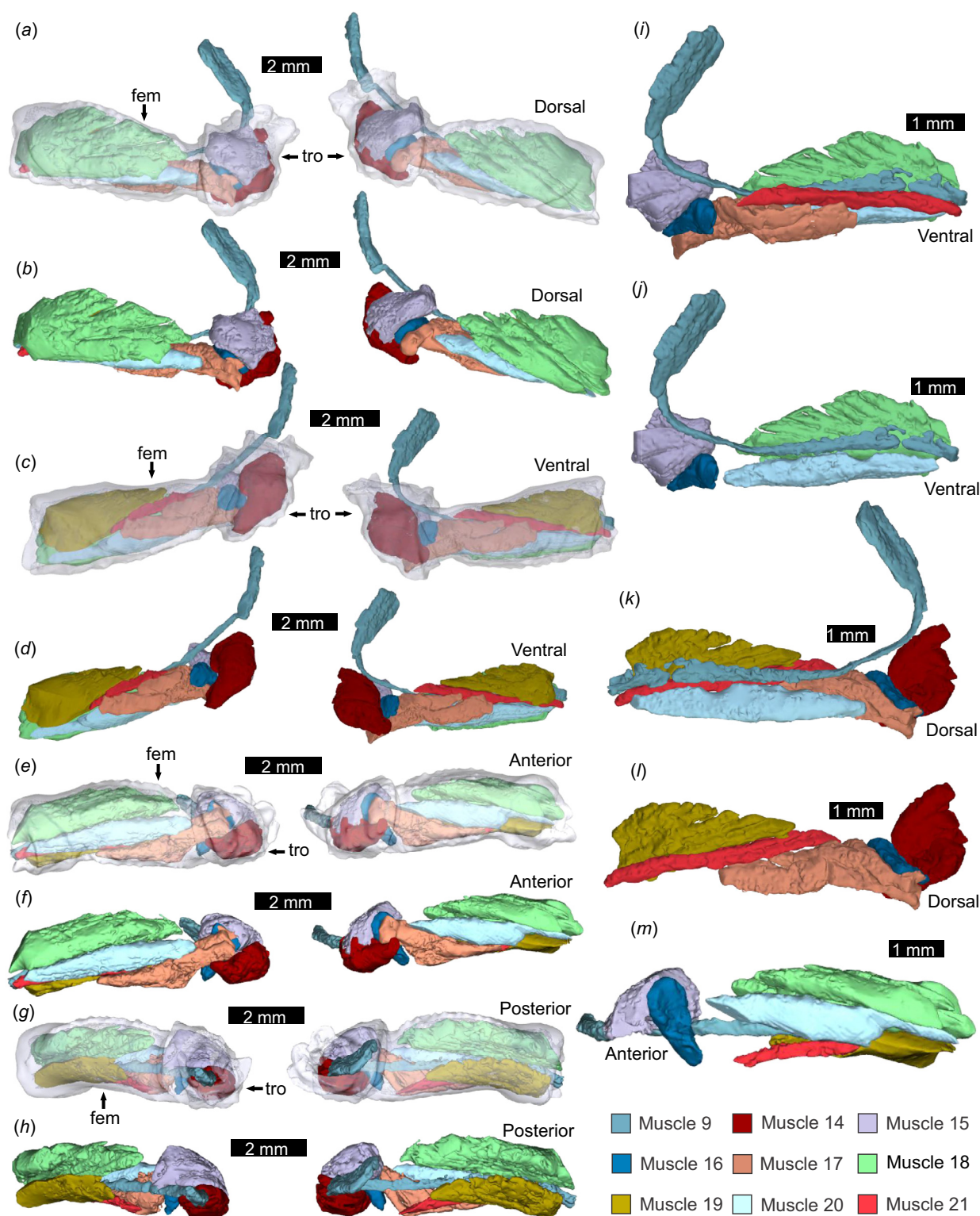


Fig. 7. Pedipalp muscles of the trochanter and femur, as modelled from micro-CT scanning. NEHM-AR-00015. (a, c, e, g) Trochanter and femur transparent with muscles. (b, d, f, h–m) Muscles without the exoskeleton. (a, b) Dorsal view. (c, d) Ventral view. (e, f) Anterior view. (g, h) Posterior view. (i, j) Ventral view of right appendage showing digital dissection of superimposed muscles. (k, l) Dorsal view of right appendage showing digital dissection of superimposed muscles. (m) Anterior view of left appendage showing digital removal of Muscles 14 and 17. Abbreviations: fem: femur; tro: trochanter. The 3D PDF associated with this reconstruction is found in Supplemental Fig. 1.

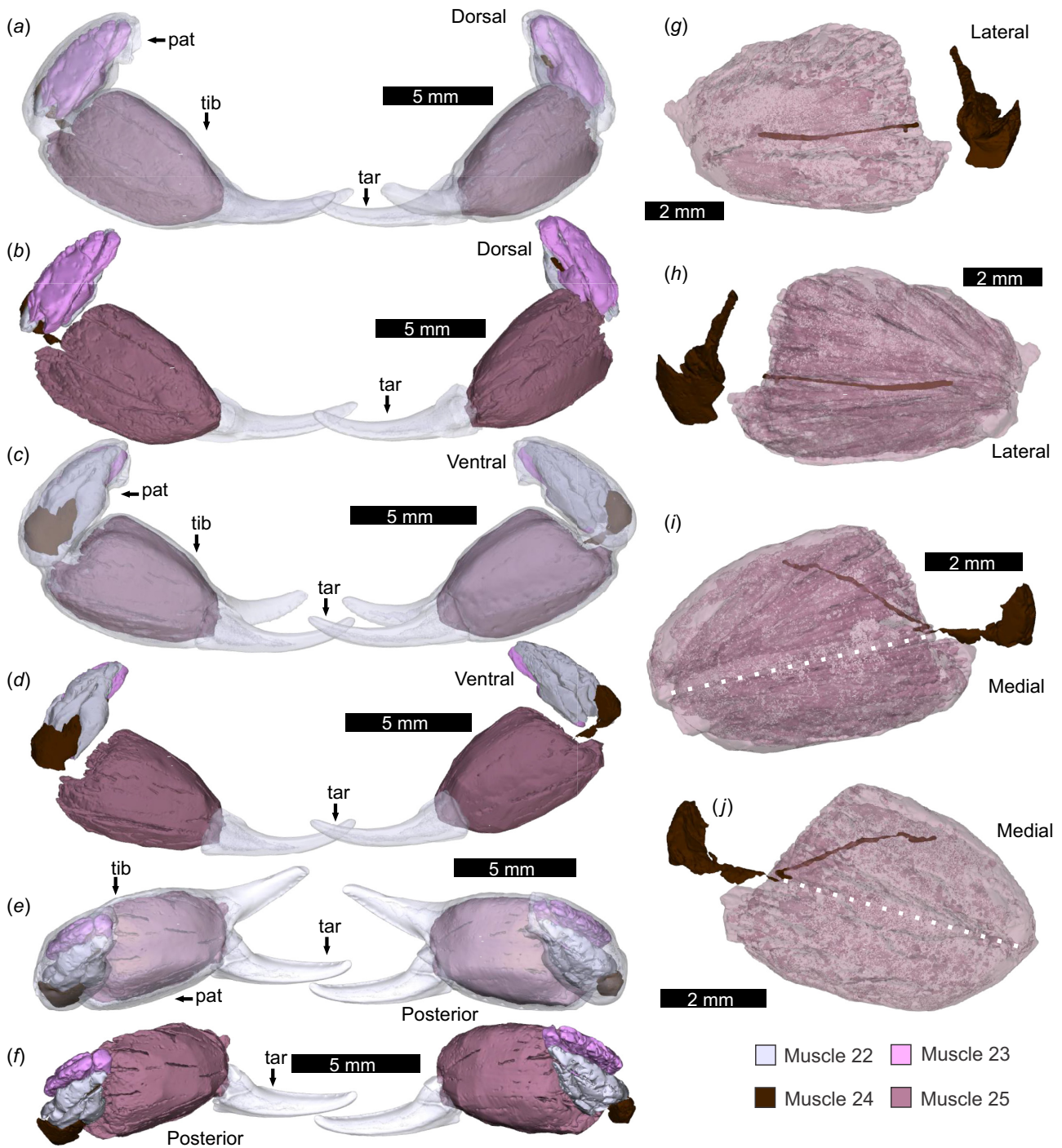


Fig. 8. Pedipalp muscles from the patella, tibia, and tarsus, as modelled from micro-CT scanning. NEHM-AR-00015. (a, c, e) Patella, tibia, and tarsus transparent with muscles. (b, d, f) Patella, tibia, and tarsus muscles with transparent tarsus. (a, b) Dorsal view. (c, d) Ventral view. (e, f) Posterior view. (g–j) Muscles 24 and 25 without the exoskeleton showing Muscle 25 as transparent. Dashed white line indicates the direction of Muscle 24. (g, h) Left appendage. (i, j) Right appendage. (g, i) Lateral view. (h, j) Medial view. Abbreviations: pat: patella; tar: tarsus; tib: tibia. The 3D PDF associated with this reconstruction is found in Supplemental Fig. 1.

Documenting pedipalp muscles of other scorpion species in 3D to build on our data may be useful for uncovering possible anatomical conservation in scorpions. Examining metasomal muscles of different scorpion genera in this framework has

shown how modifying metasomal segment morphologies impacts muscle shape, but conserves muscle groups (Günther *et al.* 2021a, 2021b). A similar situation is expected for pedipalp muscles. However, as scorpion chelae are extremely

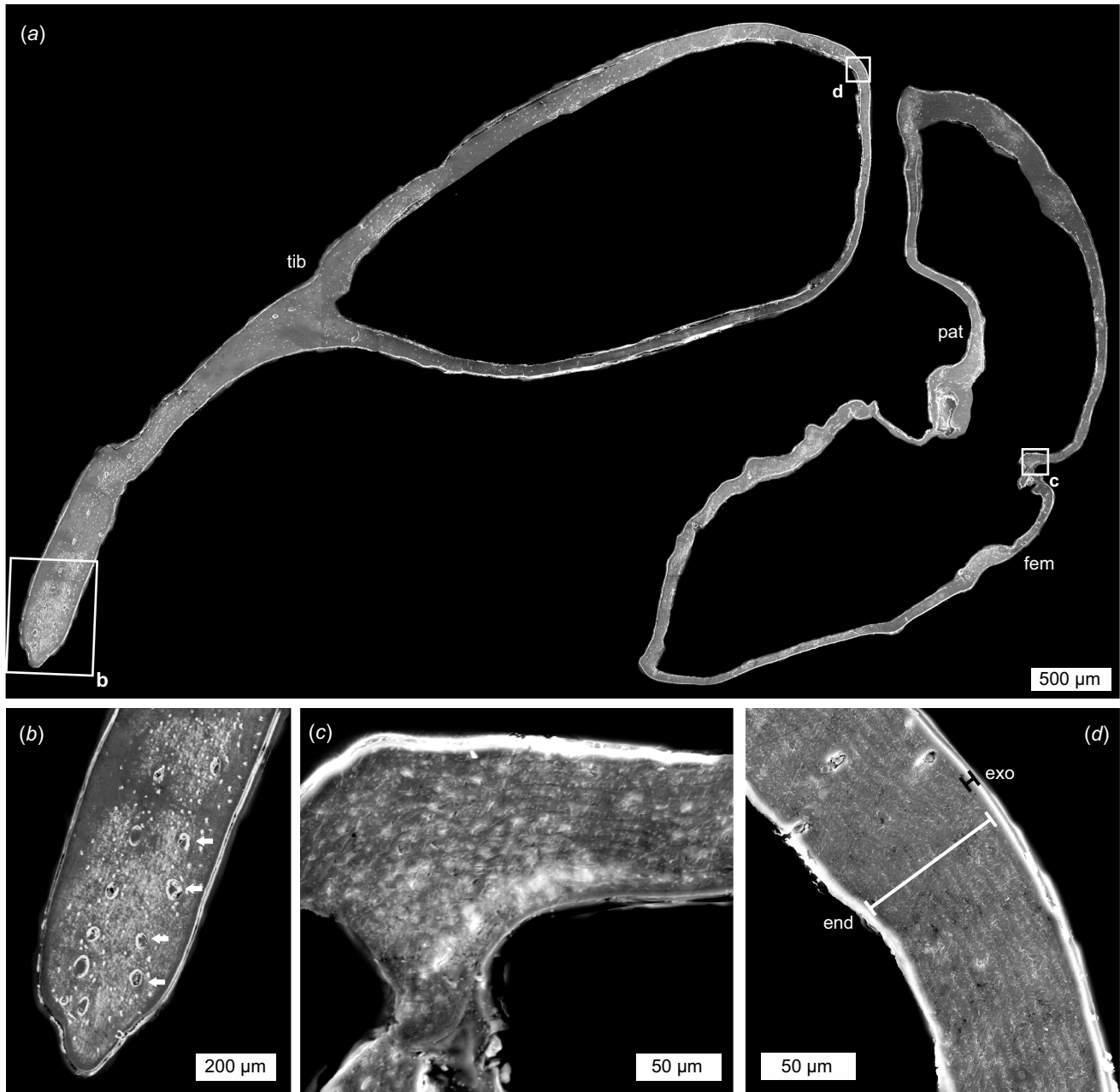


Fig. 9. SEM-SE images of a sagittal section of the pedipalp. NEHM-AR-00017. (a) Section through the femur, patella, and tibia regions; boxes outline the three areas illustrated in *b–d*. (b) Section of fixed tibia finger. Note limited laminate cuticle and extensive pore canals (white arrows). (c) Close-up of articulation between patella and femur showing laminate endocuticle. (d) Close-up of the proximal tibia edge showing laminate endocuticle (white line) and thin exocuticle (black line). The white outermost layer is epoxy resin, not cuticle. Abbreviations: end: endocuticle; exo: exocuticle; fem: femur; pat: patella; tib: tibia.

morphologically diverse (van der Meijden *et al.* 2010, 2012a; Simone and van der Meijden 2018; Bicknell *et al.* 2022), modifications to distal pedipalp muscles are likely. Such muscle data represent as-yet unexplored ecological and phylogenetic signals.

Microstructure of the chelae

Our observations of the cuticular microstructure align with previous research (Mutvei 1978; Kellersztein *et al.* 2019;

Zhang *et al.* 2023), demonstrating common cuticle construction across scorpion chelae. Among the microstructures we observed, the dorsoventrally oriented mesocuticle laminae has been noted only within the chelae and walking legs (Zhang *et al.* 2023). This modified cuticle provides reinforcement by orienting cuticle in the same direction as the maximum force, similar to the vertically oriented cuticle in *Limulus polyphemus* (Linnaeus 1758) gnathobases

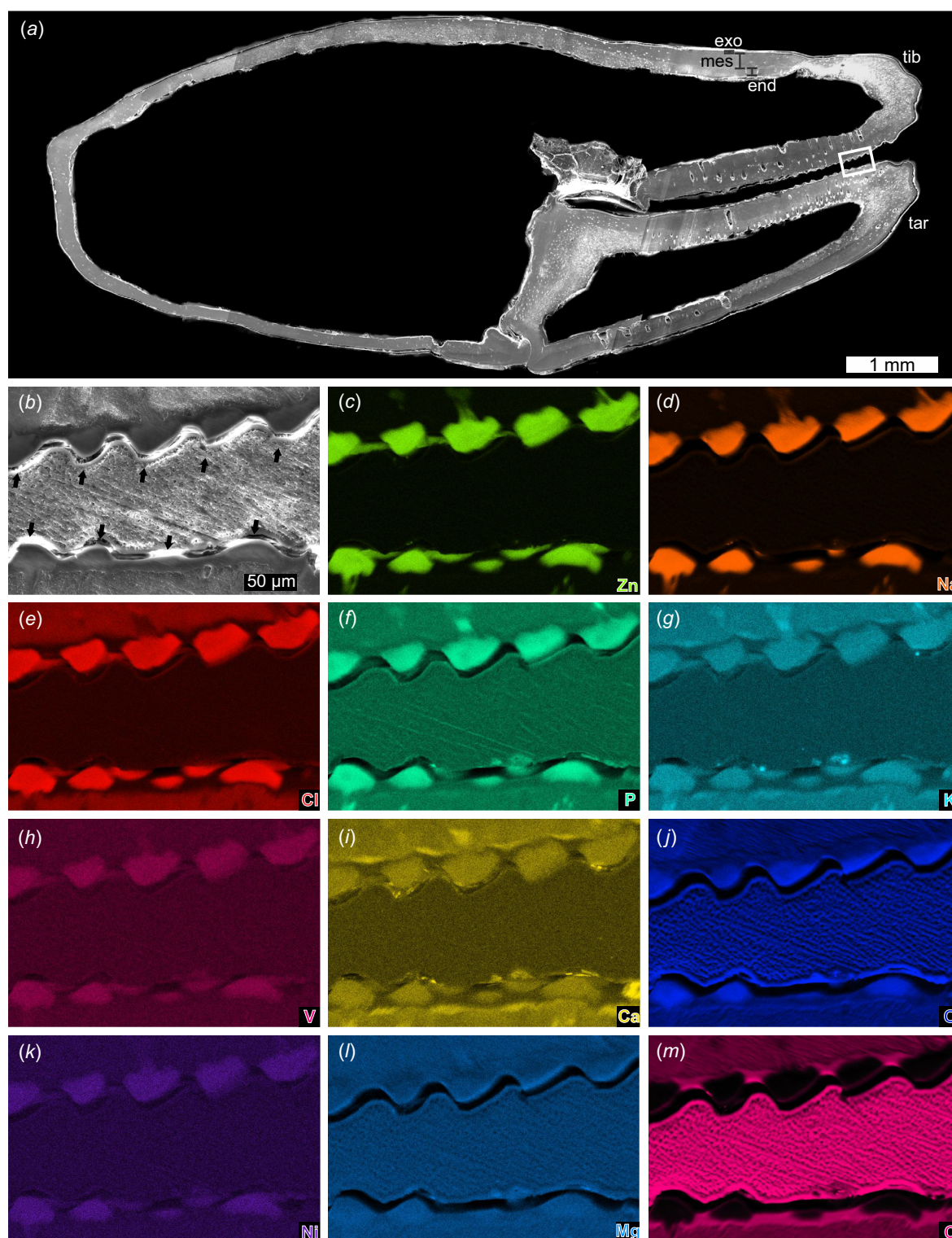


Fig. 10. SEM images and EDS elemental maps of coronal section of chela. NEHM-AR-00018. (a) SEM image of sectioned tibia and tarsus showing pore canals in the moveable and fixed fingers. Lines show cuticle section thickness. Box outlines close up in (b–m). (b) Backscatter image of box in (a) showing teeth (black arrows). (c–m) Elemental maps of zinc, sodium, chlorine, phosphorous, potassium, vanadium, calcium, oxygen, nickel, magnesium, and carbon, respectively. Note the teeth roots in (c–g). Scale bar in (b) is the same for (c–m). Abbreviations: end: endocuticle; exo: exocuticle; mes: mesocuticle; tib: tibia; tar: tarsus.

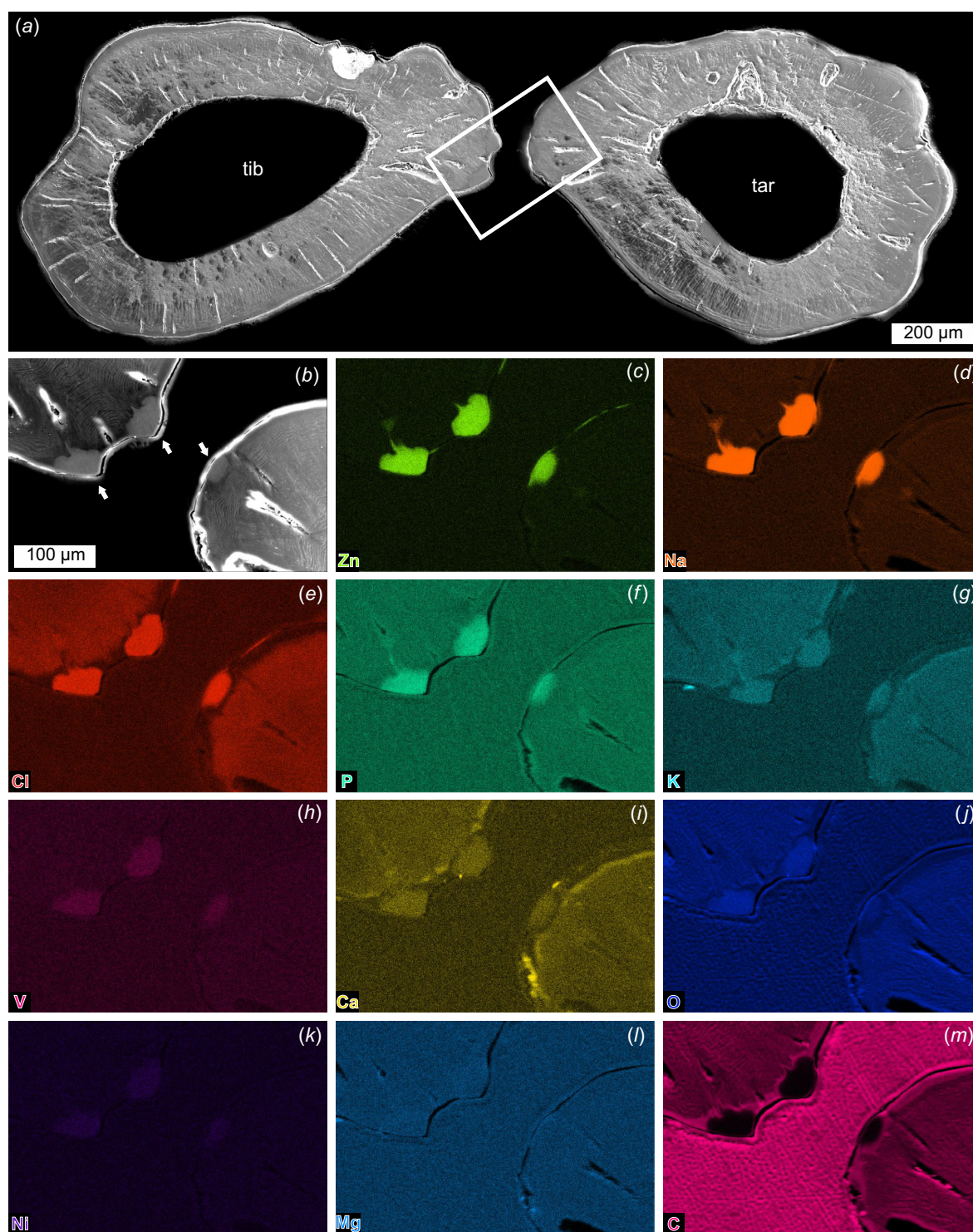


Fig. 11. SEM images and EDS elemental maps of transverse section of chela. NEHM-AR-00019. (a) SEM image of sectioned tibia and tarsus fingers showing endocuticle, mesocuticle, and pore canals. Box outlines close up in (b–m). (b) Backscatter image of box in (a) showing teeth (white arrows). (c–m) Elemental maps of zinc, sodium, chlorine, phosphorous, potassium, vanadium, calcium, oxygen, nickel, magnesium, and carbon, respectively. Scale bar in (b) is the same for (c–m). Abbreviations: end, endocuticle; exo, exocuticle; mes, mesocuticle; tib, tibia; tar, tarsus.

(Bicknell *et al.* 2018b). This increases chelae robustness overall.

Mechanical and functional interpretations can be derived by considering the three main cuticle layers. The presence

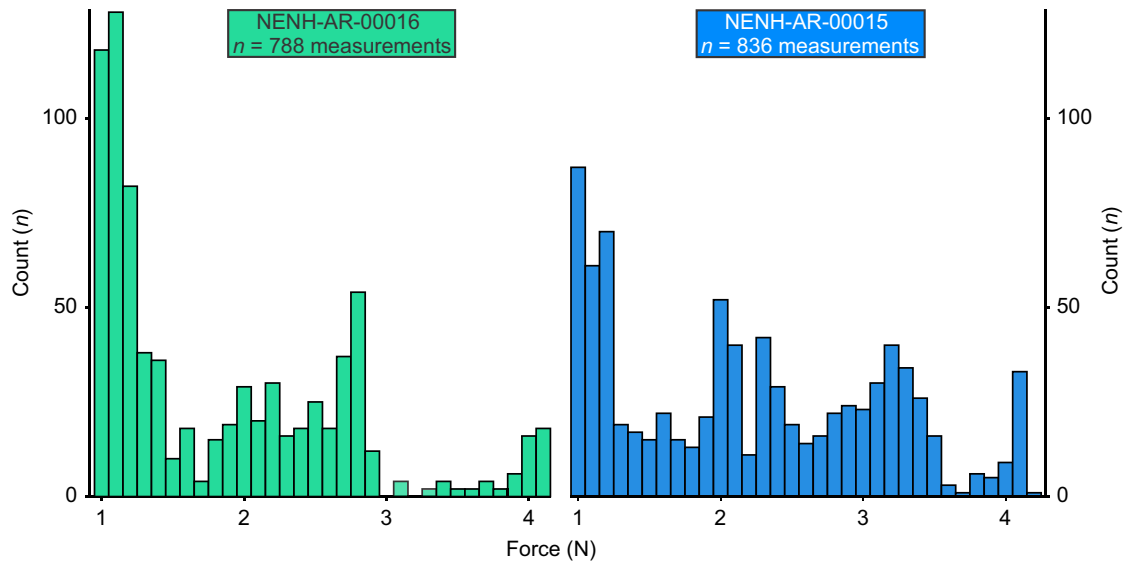


Fig. 12. Histogram plots of pinch force values for *Urodacus manicatus*. Data associated with these plots are found in Supplemental Data 2.

of these layers in the coronal and transverse orientations demonstrates how the *Urodacus manicatus* chela cuticle is constructed to experience higher stresses and strains (Kellersztein *et al.* 2019). The marked thickness of the endo- and mesocuticle, compared to the exocuticle, permits more plastic deformation within the structure, allowing for higher loads to be tolerated (Zhang *et al.* 2023). The thick endocuticle in the sagittal orientation illustrates that chelae fingers are reinforced to limit development of cracks within the cuticle (Zhang *et al.* 2023). These observations illustrate that *U. manicatus* chelae are well adapted for handling prey (Farley 1999; Simone and van der Meijden 2018; Kellersztein *et al.* 2019).

Examination of cuticle microstructure here failed to differentiate exocuticle into hyaline and inner exocuticle regions – the two main divisions of scorpion exocuticle (Filshie and Hadley 1979; Dalingwater 1987; Rubin *et al.* 2017). This likely results from our study of unstained specimens. Staining, such as Mallory's Triple Stain technique (Mallory 1900) involves the use of heavy-metal acids (e.g. phosphotungstic acid). We avoided this technique, as it would have impacted the results of the elemental mapping. However, the fluorescence of *Urodacus manicatus* under UV light (Fig. 1b) confirms the expected presence of hyaline exocuticle (Rubin *et al.* 2017).

Elemental composition of the chelae

Elemental mapping revealed several heavy elements in the cuticle. Many arthropods utilise heavy elements to reinforce cuticular structures used in food processing, such as mandibles and raptorial appendages (Hillerton *et al.* 1984; Fontaine *et al.* 1991; Schofield *et al.* 2002, 2021; Lichtenegger *et al.* 2003; Morgan *et al.* 2003; Cribb *et al.* 2008; Gallant and Hochberg

2017; Bentov *et al.* 2021). Zinc functions as a cross-linker of different proteins to increase hardness and provide reinforcement (Lichtenegger *et al.* 2003; Cribb *et al.* 2008, 2010; Gallant *et al.* 2016), allowing for higher mechanical loads (Tadayon *et al.* 2020). Increased zinc abundance in arachnids is thus far limited to chelicerae and pedipalp regions (Schofield *et al.* 1989; Schofield 2001; Cutler and McCutchen 2006; Politi *et al.* 2012; Gallant *et al.* 2016; Gallant and Hochberg 2017; Radosavljevic *et al.* 2021) and is associated with cuticle hardening for handling prey and interacting with substrate (Radosavljevic *et al.* 2021). Here, the increased zinc in *Urodacus manicatus* chelate teeth demonstrates similarly robust cuticle. A comparable abundance of chlorine in teeth reflects the presence of chlorides bonded to zinc (Hillerton and Vincent 1982; Schofield 2001; Politi *et al.* 2012) – a condition already known in scorpions (Schofield *et al.* 2003; Radosavljevic *et al.* 2021). The lack of iron within the pedipalps, as observed in the initial scans, reflects a similar pattern of enriched zinc and paucity of iron in non-buthid scorpions (Schofield 2001). The other very abundant element was sodium. However, as NaK and ZnL shell energies overlap (Radosavljevic *et al.* 2021), the presence of sodium records the overlap of energy shells, not a true abundance. Finally, nickel, potassium, and vanadium may reflect similar reinforcement as zinc in the teeth (Gallant *et al.* 2016), but their lower abundances likely demonstrate limited involvement in the hardening process.

Phosphorus is uncommon within terrestrial chelicerate cuticle (Cutler and McCutchen 2006; Gallant *et al.* 2016). When present, phosphorus is incorporated as calcium phosphate [$\text{Ca}_3(\text{PO}_4)_2$] (Currey *et al.* 1982; Becker *et al.* 2005; Gallant *et al.* 2016). As we observed phosphorus and calcium in the teeth and roots (Fig. 10f, i), the presence of calcium

phosphate seems likely. An alternative form of calcium in the cuticle is calcium oxalate (CaC_2O_4) (Norton and Behan-Pelletier 1991; Gallant and Hochberg 2017). However, the lack of carbon in roots and teeth (Figs 10*m*, 11*m*) excludes this possibility. Calcium has been documented only in spider and whip scorpion exoskeletons (Schofield *et al.* 2003; Radosavljevic *et al.* 2021). The record here suggests that calcium is likely more abundant in the chelicerate exoskeleton than previously realised.

The pathway for incorporating additional elements into exoskeletal structures is worth considering, as these elements are very uncommon within other exoskeletal regions. Heavier and otherwise uncommon elements are obtained through diet (Vohland *et al.* 2003; Gallant and Hochberg 2017) or the environment (Schofield 2001) and incorporated into the exocuticle either during sclerotisation (Cribb *et al.* 2010) or, in the case of zinc, after sclerotisation (Schofield *et al.* 2002). The process of incorporating these elements into the teeth is likely related to the roots – these structures are defined by an abundance of zinc, sodium, phosphorus, and potassium (Figs 10*c*, *d*, *f*, *g* and 11*c*, *d*, *f*, *g*), with limited vanadium and calcium (Fig. 10*h*, *i*). It seems likely that tooth roots allow zinc and other elements to move through the cuticle after sclerotisation (Schofield *et al.* 2003).

The elemental distributions demonstrate how teeth of *Urodacus manicatus* chelae are reinforced with different elements and compounds. Metal elements such as zinc, nickel, potassium, and vanadium within the teeth illustrate that they are present to decrease wear and increase the resistance to localised force. This aligns with the three main cuticle layers oriented for more plastic deformation to limit cracks developing within the cuticle during use. Taken together, the teeth and surrounding cuticular region on the chelae are reinforced for functions such as burrowing, mating, or prey capture (Kellersztein *et al.* 2021).

Most research considering the elemental construction of arthropod cuticle has employed spectrograms of specified regions (e.g. Cribb *et al.* 2008; Gallant *et al.* 2016; Gallant and Hochberg 2017; Radosavljevic *et al.* 2021). This approach uncovers an overall chemical signal but fails to demonstrate elemental distribution. By mapping elements using EDS, a thorough depiction of elemental concentrations in different regions can be determined, and structures such as the teeth roots can be detected (see also Schofield *et al.* 1989, 2002; Fawke *et al.* 1997; Politi *et al.* 2012; Tadayon *et al.* 2020; Bentov *et al.* 2021). While EDS mapping is more time-consuming than spectrograms, it presents a more detailed illustration of element location.

Urodacus manicatus pinch force and ecology

Scorpion chelae have disparate functions, the most common of which are burrowing, mating, prey capture, and occasional prey termination (van der Meijden *et al.* 2012*a*; Kellersztein *et al.* 2021; Bicknell *et al.* 2022). The strongest *Urodacus*

manicatus chelae pinch force values (4.16 N, Supplemental Data 2) are comparable to those of the African fat-tail scorpion [*Androctonus amoreuxi* (Audouin 1826)] (4.4 N) and the yellow forest scorpion [*Opisthophthalmus boehmi* (Kraepelin 1896)] (4.4 N) (Bicknell *et al.* 2022; Supplemental Table 3), both of which have chelae used for defence and predation (van der Meijden *et al.* 2010, 2013), although we acknowledge that comparison is complicated by differences in animal size. Combined with the robust morphology and the array of adaptations within the cuticular microstructure and elemental composition, this high pinch force suggests that *U. manicatus* likely uses its chelae to attack, capture, and crush prey. This contrasts with forms that display lower force values (<1 N) and rapid chelae closing speeds, using the chelae to hold prey for incapacitation by the stinger (Casper 1985; van der Meijden *et al.* 2013; Simone and van der Meijden 2018). This observation also aligns with the life mode of *U. manicatus* as a predator that waits at burrow entrances for prey (Holden 1997) and uses pedipalps, rather than the stinger, to initially subdue prey (Simone and van der Meijden 2018).

A major complication in attempting to more thoroughly understand scorpion feeding ecology is the infrequent consumption of prey (Simone and van der Meijden 2021). *Urodacus manicatus*, in particular, can survive for up to eight months without food (Southcott 1955). As such, our morphofunctional interpretations of predation are not supported by behavioural observations. However, the application of chelae to subdue prey aligns with the substantial reinforcement of chelate teeth with metals, the additional mesocuticle, and a large tarsal muscle. Field studies of this and other scorpion species, supplemented by metabarcoding of gut contents (Simone *et al.* 2022), are required to validate these proposed ecological hypotheses.

Synthesis of methodologies

The examination of one biological structure using four methods has given insight into the morphofunctionality of *Urodacus manicatus* and, more broadly, offers an integrated framework for exploring a key predatory adaptation. Pedipalp musculature is more elaborate than previously noted, including multiple muscles used in prey capture and manipulation. The microstructural data show how thick chelae endo- and mesocuticle allow for plastic deformation, while promoting robustness for enduring increased force during predation. This is supported by the high concentration of metals within the chelae teeth that likely reduce the wear these regions experience. Finally, the force data allow us to contextualise the mechanical performance compared to other species, while ground-truthing the microstructural and skeletomuscular data. Together, these adaptations and morphologies result in a biological structure employed in prey capture and processing.

Future directions

The synthetic approach to understanding *Urodacus manicatus* presented here forms a base for developing research on this species, and for scorpions more broadly. During this research, we identified three main future directions that are important for expanding on this line of enquiry:

- (1) *Homology and variation of scorpion appendage muscles*: To better understand scorpion pedipalp muscles more broadly, detailed examination of other scorpion species is needed. Building on Günther *et al.* (2021b), micro-CT scans and segmentation of species from other families will uncover the location and morphology of muscles that could inform on patterns in muscle evolution. Documentation of walking leg muscles would provide the data needed to test homology statements tentatively outlined here.
- (2) *Metals in chelae teeth*: It is interesting to consider how uncommon elements, such as vanadium, have been sequestered into the scorpion exoskeleton and, furthermore, to examine if this condition is common across Scorpiones. We propose two approaches to explore these ideas: (a) Modification of diet under controlled conditions to see if consumption of different prey items affects elemental concentrations in the chelae teeth, building on Schofield (2001); (b) More comprehensive documentation of elemental concentrations within chelae teeth across Scorpiones to explore phylogenetic trends associated with composition (Schofield 2001).
- (3) *Black Rock Scorpion ecology*: Most research focusing on *Urodacus manicatus* biology has considered burrowing (Woodman 2008), reproduction (Southcott 1955; Warburg and Rosenberg 1994), toxicology (Lowe and Farrell 2011; Luna-Ramirez *et al.* 2017), and overall physiology (Holden 1997). There is little information on how the species subdues prey. To build on the pinch force analyses presented here, we propose that continued examination into *U. manicatus* predatory behaviours will further contextualise the force data and, more broadly, the morphofunctional synthesis presented here.

Supplementary material

Supplementary material is available [online](#).

References

- Abdel-Nabi IM, McVean A, Abdel-Rahman MA, Omran M (2004) Intraspecific diversity of morphological characters of the burrowing scorpion *Scorpio maurus palmatus* (Ehrenberg, 1828) in Egypt (Arachnida: Scorpionida: Scorpionidae). *Serket* 9(2), 41–67.
- Alexander AJ (1967) Problems of limb extension in the scorpion, *Opisthophthalmus latimanus* Koch. *Transactions of the Royal Society of South Africa* 37(3), 165–181. doi:10.1080/00359196709519065
- Audouin JV (1826) Explication sommaire des planches d'araignées de l'Égypte et de la Syrie. In 'Description de l'Égypte'. Vol. 22. (Ed. J-C Savigny) pp. 291–430. (Histoire Naturelle: Paris)
- Beck EJ (1885) Description of the muscular and endoskeletal systems of *Scorpio*. *Transactions of the Zoological Society of London* 11, 339–360.
- Becker A, Ziegler A, Epple M (2005) The mineral phase in the cuticles of two species of Crustacea consists of magnesium calcite, amorphous calcium carbonate, and amorphous calcium phosphate. *Dalton Transactions* 10, 1814–1820. doi:10.1039/b412062k
- Bentov S, Palmer BA, Bar-On B, Shelef Y, Aflalo ED, Sagi A (2021) Reinforcement of bio-apatite by zinc substitution in the incisor tooth of a prawn. *Acta Biomaterialia* 120, 116–123. doi:10.1016/j.actbio.2020.07.039
- Bicknell RDC, Klinkhamer AJ, Flavel RJ, Wroe S, Paterson JR (2018a) A 3D anatomical atlas of appendage musculature in the chelicerate arthropod *Limulus polyphemus*. *PLoS ONE* 13(2), e0191400. doi:10.1371/journal.pone.0191400
- Bicknell RDC, Paterson JR, Caron J-B, Skovsted CB (2018b) The gnathobasic spine microstructure of recent and Silurian chelicerates and the Cambrian artiopodan *Sidneyia*: functional and evolutionary implications. *Arthropod Structure & Development* 47(1), 12–24. doi:10.1016/j.asd.2017.12.001
- Bicknell RDC, Simone Y, van der Meijden A, Wroe S, Edgecombe GD, Paterson JR (2022) Biomechanical analyses of pterygotid sea scorpion chelicerae uncover predatory specialisation within eurypterids. *PeerJ* 10, e14515. doi:10.7717/peerj.14515
- Bowerman RF, Root TM (1978) External anatomy and muscle morphology of the walking legs of the scorpion *Hadrurus arizonensis*. *Comparative Biochemistry and Physiology Part A: Physiology* 59(1), 57–63. doi:10.1016/0300-9629(78)90306-7
- Casper GS (1985) Prey capture and stinging behavior in the emperor scorpion, *Pandinus imperator* (Koch) (Scorpiones, Scorpionidae). *The Journal of Arachnology* 13, 277–283.
- Cribb BW, Stewart A, Huang H, Truss R, Noller B, Rasch R, Zalucki MP (2008) Unique zinc mass in mandibles separates drywood termites from other groups of termites. *Naturwissenschaften* 95(5), 433–441. doi:10.1007/s00114-008-0346-3
- Cribb BW, Lin C-L, Rintoul L, Rasch R, Hasenpusch J, Huang H (2010) Hardness in arthropod exoskeletons in the absence of transition metals. *Acta Biomaterialia* 6(8), 3152–3156. doi:10.1016/j.actbio.2010.02.009
- Cunha HP, Santos AB, Foerster SIA, Moura GJB, Lira AFA (2022) Can contrasting habitats influence predatory behavior in tropical forest scorpions? *Acta Ethologica* 25(2), 107–113. doi:10.1007/s10211-022-00390-5
- Currey JD, Nash A, Bonfield W (1982) Calcified cuticle in the stomatopod smashing limb. *Journal of Materials Science* 17(7), 1939–1944. doi:10.1007/BF00540410
- Cutler B, McCutchen L (2006) Heavy metals in cuticular structures of Palpigradi, Ricinulei, and Schizomida (Arachnida). *The Journal of Arachnology* 34(3), 653–656. doi:10.1636/S05-37.1
- Dalingwater JE (1987) Chelicerate cuticle structure. In 'Ecophysiology of Spiders'. (Ed. W Nentwig) pp. 3–15. (Springer: Berlin)
- Durale MS, Vyas AB (1968) The structure of the chela of *Heterometrus* sp. and its mode of operation. *Bulletin of the Southern California Academy of Sciences* 67(4), 240–244.
- Ehrenberg CG (1828) Phytozoa turbellaria Africana et Asiatica in Phytozoorum Tabula IV et V delineata. In 'Symbolae physicae, seu icones et descriptiones corporum naturalium novorum aut minus cognitorum quae ex itineribus per Libyam, Aegyptium, Nubiam, Dongalam Syriam, Arabiam et Habessiniam, pars zoologica II, animalia evertibrata exclusis insectis'. (Eds FG Hemprich, CG Ehrenberg) pp. 53–67. (Officina Academica: Berolina)
- Farley RD (1999) Scorpiones. In 'Microscopic anatomy of invertebrates. Vol. 8A: Chelicerate arthropods'. (Eds FW Harrison, RF Foelix) pp. 117–222. (Wiley-Liss: New York)
- Fawke JD, McClements JG, Wyeth P (1997) Cuticular metals: quantification and mapping by complementary techniques. *Cell Biology International* 21(10), 675–678. doi:10.1006/cbir.1998.0166
- Filshie BK, Hadley NF (1979) Fine structure of the cuticle of the desert scorpion, *Hadrurus arizonensis*. *Tissue and Cell* 11(2), 249–262. doi:10.1016/0040-8166(79)90040-5

- Fontaine AR, Olsen N, Ring RA, Singla CL (1991) Cuticular metal hardening of mouthparts and claws of some forest insects of British Columbia. *Journal of the Entomological Society of British Columbia* **88**, 45–55.
- Gainett G, Klementz BC, Setton EVW, Simian C, Iuri H, Edgcombe GD, Peretti AV, Sharma PP (2024) A plurality of morphological characters need not equate with phylogenetic accuracy: a rare genomic change refutes the placement of Solifugae and Pseudoscorpiones in Haplocnemata. *Evolution and Development* e12467. doi:10.1111/ede.12467
- Gallant J, Hochberg R (2017) Elemental characterization of the exoskeleton in the whipscorpions *Mastigoproctus giganteus* and *Typopeltis dalyi* (Arachnida: Thelyphonida). *Invertebrate Biology* **136**(3), 345–359. doi:10.1111/ivb.12187
- Gallant J, Hochberg R, Ada E (2016) Elemental characterization of the cuticle in the marine intertidal pseudoscorpion, *Halobisium occidentale*. *Invertebrate Biology* **135**(2), 127–137. doi:10.1111/ivb.12123
- Gignac PM, Kley NJ, Clarke JA, Colbert MW, Morhardt AC, Cerio D, Cost IN, Cox PG, Daza JD, Early CM, Echols MS, Henkelman RM, Herdina AN, Holliday CM, Li Z, Mahlow K, Merchant S, Müller J, Orsbon CP, Paluh DJ, Thies ML, Tsai HP, Witmer LM (2016) Diffusible iodine-based contrast-enhanced computed tomography (diceCT): an emerging tool for rapid, high-resolution, 3-D imaging of metazoan soft tissues. *Journal of Anatomy* **228**, 889–909. doi:10.1111/joa.12449
- Grams M, Wirkner CS, Runge J (2018) Serial and special: comparison of podomeres and muscles in tactile vs walking legs of whip scorpions (Arachnida, Uropygi). *Zoologischer Anzeiger* **273**, 75–101. doi:10.1016/j.jcz.2017.06.001
- Günther A, Drack M, Monod L, Wirkner CS (2021a) A unique yet technically simple type of joint allows for the high mobility of scorpion tails. *Journal of the Royal Society Interface* **18**(182), 20210388. doi:10.1098/rsif.2021.0388
- Günther A, Monod L, Wirkner CS (2021b) Comparative morphology of scorpion metasomata: Muscles and cuticle. *Arthropod Structure & Development* **60**, 101003. doi:10.1016/j.asd.2020.101003
- Harington A (1977) Burrowing biology of the scorpion *Cheloctonus jonesii* Pocock (Arachnida: Scorpionida: Scorpionidae). *Journal of Arachnology* **5**, 243–249.
- Harvey MS, Volschenk ES (2002) A forgotten scorpion: the identity of *Buthus flavicuris* Rainbow, 1896 (Scorpiones), with notes on *Urodacus manicatus* (Thorell). *Records of the Western Australian Museum* **21**(1), 105–106. doi:10.18195/issn.0312-3162.21(1).2002.105-106
- Hillerton JE, Vincent JFV (1982) The specific location of zinc in insect mandibles. *Journal of Experimental Biology* **101**, 333–336. doi:10.1242/jeb.101.1.333
- Hillerton JE, Robertson B, Vincent JFV (1984) The presence of zinc or manganese as the predominant metal in the mandibles of adult, stored-product beetles. *Journal of Stored Products Research* **20**(3), 133–137. doi:10.1016/0022-474X(84)90020-1
- Holden C (1997) The environmental physiology of the scorpion *Urodacus manicatus* (Thorell) (Scorpionidae). PhD thesis, University of New England.
- Kellersztein I, Cohen SR, Bar-On B, Wagner HD (2019) The exoskeleton of scorpions' pincers: structure and micro-mechanical properties. *Acta Biomaterialia* **94**, 565–573. doi:10.1016/j.actbio.2019.06.036
- Kellersztein I, Greenfeld I, Wagner HD (2021) Structural analysis across length scales of the scorpion pincer cuticle. *Bioinspiration & Biomimetics* **16**(2), 026013. doi:10.1088/1748-3190/abd2d2
- Kennaugh J (1959) An examination of the cuticles of two scorpions, *Pandinus imperator* and *Scorpiops hardwickii*. *Journal of Cell Science* **S3**-100(49), 41–50. doi:10.1242/jcs.s3-100.49.41
- Koch CL (1837) 'Übersicht des Arachnidensystems. Erstes Heft.' (C. H. Zeh'schen Buchhandlung: Nürnberg)
- Koch LE (1978) A comparative study of the structure, function and adaptation to different habitats of burrows in the scorpion genus *Urodacus* (Scorpionida, Scorpionidae). *Records of the Western Australian Museum* **6**(2), 119–146.
- Kraepelin K (1896) Neue und weniger bekannte Scorpione. *Mitteilungen aus dem Naturhistorischen Museum (Mitteilungen aus dem Naturhistorischen Museum (Beiheft zum Jahrbuch der Hamburgischen Wissenschaftlichen Anstalten))* **13**, 119–146.
- Krishnan G (1953) On the cuticle of the scorpion *Palamneus swammerdami*. *Journal of Cell Science* **S3**-94(25), 11–22. doi:10.1242/jcs.s3-94.25.11
- Lamoral BH (1971) Predation on terrestrial molluscs by scorpions in the Kalahari Desert. *Annals of the Natal Museum* **21**(1), 17–20.
- Lanckster ER (1885) On the muscular and endoskeletal systems of *Limulus* and *Scorpio*; with some notes on the anatomy and generic characters of scorpions. *The Transactions of the Zoological Society of London* **11**(10), 311–384. doi:10.1111/j.1096-3642.1885.tb00346.x
- Leeming J (2019) 'Scorpions of southern Africa.' (Penguin Random House: South Africa)
- Lichtenegger HC, Schöberl T, Ruokolainen JT, Cross JO, Heald SM, Birkedal H, Waite JH, Stucky GD (2003) Zinc and mechanical prowess in the jaws of *Nereis*, a marine worm. *Proceedings of the National Academy of Sciences* **100**(16), 9144–9149.
- Linnaeus C (1758) 'Systema naturae per regna tria naturae, secundum classes, ordines, genera, species, cum characteribus, differentiis, synonymis, locis.' 10 edn. (Laurentius Salvius: Holmiae)
- Lowe RM, Farrell PM (2011) A portable device for the electrical extraction of scorpion venom. *Toxicon* **57**(2), 244–247. doi:10.1016/j.toxicon.2010.11.017
- Luna-Ramirez K, Tonk M, Rahnamaeian M, Vilcinskis A (2017) Bioactivity of natural and engineered antimicrobial peptides from venom of the scorpions *Urodacus yaschenkoi* and *U. manicatus*. *Toxins* **9**(1), 22. doi:10.3390/toxins9010022
- Malek SRA (1964) A study of a scorpion cuticle: I. The structure and staining reactions of the fully formed cuticle of *Buthus quinquestriatus* (H. & E.). *Proceedings of the Linnean Society of London* **175**(2), 101–116.
- Mallory FB (1900) A contribution to staining methods: I. A differential stain for connective-tissue fibrillae and reticulum. II. Chloride of iron haematoxylin for nuclei and fibrin. III. Phosphotungstic acid haematoxylin for neuroglia fibres. *Journal of Experimental Medicine* **5**(1), 15–20. doi:10.1084/jem.5.1.15
- Manton SM (1977) 'The Arthropoda: habits, functional morphology and evolution.' (Oxford University Press: Oxford)
- Metscher BD (2009) MicroCT for comparative morphology: simple staining methods allow high-contrast 3D imaging of diverse non-mineralized animal tissues. *BMC Physiology* **9**(1), 11. doi:10.1186/1472-6793-9-11
- Michalski H, Harms D, Runge J, Wirkner CS (2022) Evolutionary morphology of coxal musculature in Pseudoscorpiones (Arachnida). *Arthropod Structure & Development* **69**, 101165. doi:10.1016/j.asd.2022.101165
- Morgan TD, Baker P, Kramer KJ, Basibuyuk HH, Quicke DLJ (2003) Metals in mandibles of stored product insects: do zinc and manganese enhance the ability of larvae to infest seeds? *Journal of Stored Products Research* **39**(1), 65–75. doi:10.1016/S0022-474X(02)00019-X
- Mutvei H (1978) SEM studies on arthropod exoskeletons II. Horseshoe crab *Limulus polyphemus* (L.) in comparison with extinct eurypterids and recent scorpions. *Zoologica Scripta* **6**(3), 203–213. doi:10.1111/j.1463-6409.1978.tb00771.x
- Norton RA, Behan-Pelletier VM (1991) Calcium carbonate and calcium oxalate as cuticular hardening agents in oribatid mites (Acari: Oribatida). *Canadian Journal of Zoology* **69**(6), 1504–1511. doi:10.1139/z91-210
- Ontano AZ, Gainett G, Aharon S, Ballesteros JA, Benavides LR, Corbett KF, Gavish-Regev E, Harvey MS, Monsma S, Santibañez-López CE, Setton EVW, Zehms JT, Zeh JA, Zeh DW, Sharma PP, Pupko T (2021) Taxonomic sampling and rare genomic changes overcome long-branch attraction in the phylogenetic placement of pseudoscorpions. *Molecular Biology and Evolution* **38**(6), 2446–2467. doi:10.1093/molbev/msab038
- Pocock RI (1888) XX. – The species of the genus *Urodacus* contained in the collection of the British (Natural-History) Museum. *Annals and Magazine of Natural History* **2**(8), 169–175. doi:10.1080/00222938809460897
- Pocock RI (1898) VIII. – The Australian scorpions of the genus *Urodacus*, Pet. *Annals and Magazine of Natural History* **2**(7), 59–67. doi:10.1080/00222939808678012
- Politi Y, Prieuwater M, Pippel E, Zaslansky P, Hartmann J, Siegel S, Li C, Barth FG, Fratzl P (2012) A spider's fang: how to design an injection needle using chitin-based composite material. *Advanced Functional Materials* **22**(12), 2519–2528. doi:10.1002/adfm.201200063
- Radosavljevic D, Ada E, Hochberg R (2021) Elemental enrichment of the exoskeleton of the whip spider *Phrynos marginemaculatus* (Arachnida:

- Amblypygi). *The Journal of Arachnology* 49(2), 235–249. doi:10.1636/JoA-S-20-048
- Richards AC (1951) 'Integument of Arthropods.' (University of Minnesota Press: Minneapolis)
- Rubin M, Lamsdell JC, Prendini L, Hopkins MJ (2017) Exocuticular hyaline layer of sea scorpions and horseshoe crabs suggests cuticular fluorescence is plesiomorphic in chelicerates. *Journal of Zoology* 303(4), 245–253. doi:10.1111/jzo.12493
- Runge J, Wirkner CS (2020) Evolutionary and functional substitution of extrinsic musculature in Solifugae (Arachnida). *Journal of Morphology* 281(12), 1524–1533. doi:10.1002/jmor.21260
- Schmidt M, Melzer RR, Bicknell RDC (2022) Kinematics of whip spider pedipalps: a 3D comparative morpho-functional approach. *Integrative Zoology* 17(1), 156–167. doi:10.1111/1749-4877.12591
- Schofield RMS (2001) Metals in cuticular structures. In 'Scorpion biology and research.' (Eds P Brownell, Polis G) pp. 234–256. (Oxford University Press: Oxford)
- Schofield R, Lefevre H, Shaffer M (1989) Complementary microanalysis of Zn, Mn and Fe in the chelicera of spiders and scorpions using scanning MeV-ion and electron microprobes. *Nuclear Instruments and Methods in Physics Research Section B: Beam Interactions with Materials and Atoms* 40, 698–701. doi:10.1016/0168-583X(89)91077-X
- Schofield RMS, Nesson MH, Richardson KA (2002) Tooth hardness increases with zinc-content in mandibles of young adult leaf-cutter ants. *Naturwissenschaften* 89, 579–583. doi:10.1007/s00114-002-0381-4
- Schofield RMS, Nesson MH, Richardson KA, Wyeth P (2003) Zinc is incorporated into cuticular "tools" after ecdysis: The time course of the zinc distribution in "tools" and whole bodies of an ant and a scorpion. *Journal of Insect Physiology* 49(1), 31–44. doi:10.1016/S0022-1910(02)00224-X
- Schofield RMS, Bailey J, Coon JJ, Devaraj A, Garrett RW, Goggans MS, Hebner MG, Lee BS, Lee D, Lovern N, Ober-Singleton S, Saephan N, Seagal VR, Silver DM, Som HE, Twitchell J, Wang X, Zima JS, Nesson MH (2021) The homogenous alternative to biomineralization: Zn- and Mn-rich materials enable sharp organismal "tools" that reduce force requirements. *Scientific Reports* 11(1), 17481. doi:10.1038/s41598-021-91795-y
- Shorthouse DJ, Marples TG (1982) The life stages and population dynamics of an arid zone scorpion *Urodacus yaschenkoi* (Birula 1903). *Australian Journal of Ecology* 7(2), 109–118. doi:10.1111/j.1442-9993.1982.tb01584.x
- Shultz JW (1989) Morphology of locomotor appendages in Arachnida: evolutionary trends and phylogenetic implications. *Zoological Journal of the Linnean Society* 97(1), 1–55. doi:10.1111/j.1096-3642.1989.tb00552.x
- Shultz JW (1992) Muscle firing patterns in two arachnids using different methods of propulsive leg extension. *Journal of Experimental Biology* 162(1), 313–329. doi:10.1242/jeb.162.1.313
- Shultz JW (2001) Gross muscular anatomy of *Limulus polyphemus* (Xiphosura, Chelicerata) and its bearing on evolution in the Arachnida. *Journal of Arachnology* 29(3), 283–303. doi:10.1636/0161-8202(2001)029[0283:GMAOLP]2.0.CO;2
- Shultz JW (2007) Morphology of the prosomal endoskeleton of Scorpiones (Arachnida) and a new hypothesis for the evolution of cuticular cephalic endoskeletons in arthropods. *Arthropod Structure & Development* 36(1), 77–102. doi:10.1016/j.asd.2006.08.001
- Simone Y, van der Meijden A (2018) Fast and fine versus strong and stout: a trade-off between chela closing force and speed across nine scorpion species. *Biological Journal of the Linnean Society* 123(1), 208–217. doi:10.1093/biolinnean/blx139
- Simone Y, van der Meijden A (2021) Armed stem to stinger: a review of the ecological roles of scorpion weapons. *Journal of Venomous Animals and Toxins including Tropical Diseases* 27, e20210002. doi:10.1590/1678-9199-jvatitd-2021-0002
- Simone Y, Chaves C, van der Meijden A, Egeter B (2022) Metabarcoding analysis of different portions of the digestive tract of scorpions (Scorpiones, Arachnida) following a controlled diet regime shows long prey DNA half-life. *Environmental DNA* 4(5), 1176–1186. doi:10.1002/edn3.311
- Smith GT (1966) Observations on the life history of the scorpion *Urodacus abruptus* (Scorpionidae), and the analysis of its home sites. *Australian Journal of Zoology* 14(3), 383–398. doi:10.1071/ZO9660383
- Snodgrass RE (1948) The feeding organs of Arachnida, including mites and ticks. *Smithsonian Miscellaneous Collections* 110(10), 1–93.
- Snodgrass RE (1952) 'A textbook of arthropod anatomy.' (Cornell University Press: New York)
- Soleglad ME, Fet V, Kovařík F (2005) The systematic position of the scorpion genera *Heteroscorpion* Birula, 1903 and *Urodacus* Peters, 1861 (Scorpiones: Scorpionoidea). *Euscorpius* 2005(20), 1–37. doi:10.18590/euscorpius.2005.vol2005.iss20.1
- Southcott RV (1955) Some observations on the biology, including mating and other behavior, of the Australian scorpion *Urodacus abruptus* Pocock. *Transactions of the Royal Society of South Australia* 78, 145–154.
- Tadayon M, Younes-Metzler O, Shelef Y, Zaslansky P, Rechels A, Berner A, Zolotoyabko E, Barth FG, Fratzi P, Bar-On B (2020) Adaptations for wear resistance and damage resilience: micromechanics of spider cuticular "tools". *Advanced Functional Materials* 30(32), 2000400. doi:10.1002/adfm.202000400
- Thorell T (1876) I. – On the classification of scorpions. *Annals and Magazine of Natural History* 17(97), 1–15. doi:10.1080/00222937.608681889
- van der Meijden A, Kleinteich T (2017) A biomechanical view on stinger diversity in scorpions. *Journal of Anatomy* 230(4), 497–509. doi:10.1111/joa.12582.
- van der Meijden A, Herrel A, Summers A (2010) Comparison of chela size and pincer force in scorpions; getting a first grip. *Journal of Zoology* 280(4), 319–325. doi:10.1111/j.1469-7998.2009.00628.x
- van der Meijden A, Kleinteich T, Coelho P (2012a) Packing a pinch: functional implications of chela shapes in scorpions using finite element analysis. *Journal of Anatomy* 220(5), 423–434. doi:10.1111/j.1469-7580.2012.01485.x
- van der Meijden A, Langer F, Boistel R, Vagovic P, Heethoff M (2012b) Functional morphology and bite performance of raptorial chelicerae of camel spiders (Solifugae). *Journal of Experimental Biology* 215(19), 3411–3418. doi:10.1242/jeb.072926
- van der Meijden A, Lobo Coelho P, Sousa P, Herrel A (2013) Choose your weapon: defensive behavior is associated with morphology and performance in scorpions. *PLoS ONE* 8(11), e78955. doi:10.1371/journal.pone.0078955
- Vohland K, Furch K, Adis J (2003) Contrasting central Amazonian rainforests and their influence on chemical properties of the cuticle of two millipede species – a first study. *Tropical Ecology* 44(2), 235–241.
- Vyas AB (1970) Studies in myology of the scorpion *Heterometrus fulvipes* Koch. PhD Thesis, Gujarat University.
- Walker SM, Schwyn DA, Mokso R, Wicklein M, Müller T, Doube M, Stapanioni M, Krapp HG, Taylor GK (2014) In vivo time-resolved microtomography reveals the mechanics of the blowfly flight motor. *PLoS Biology* 12(3), e1001823. doi:10.1371/journal.pbio.1001823
- Warburg MR, Rosenberg M (1994) The female reproductive system of the eastern Australian scorpion. *Tissue and Cell* 26(5), 779–783. doi:10.1016/0040-8166(94)90060-4
- Wirkner CS, Prendini L (2007) Comparative morphology of the hemolymph vascular system in scorpions – A survey using corrosion casting, MicroCT, and 3D-reconstruction. *Journal of Morphology* 268(5), 401–413. doi:10.1002/jmor.10512
- Wolf H, Harzsch S (2002) Evolution of the arthropod neuromuscular system. 1. Arrangement of muscles and innervation in the walking legs of a scorpion: *Vaejovis spinigerus* (Wood, 1863) Vaejovidae, Scorpiones, Arachnida. *Arthropod Structure & Development* 31(3), 185–202. doi:10.1016/S1467-8039(02)00043-9
- Woodman JD (2008) Living in a shallow burrow under a rock: gas exchange and water loss in an Australian scorpion. *Journal of Thermal Biology* 33(5), 280–286. doi:10.1016/j.jtherbio.2008.02.006
- Zhang H, Kellersztain I, Freychet G, Zhernenkov M, Wagner HD, Greer JR (2023) Chemo-mechanical-microstructural coupling in the tarsus exoskeleton of the scorpion *Scorpio palmatus*. *Acta Biomaterialia* 160, 176–186. doi:10.1016/j.actbio.2023.01.038
- Zhao Z-L, Shu T, Feng X-Q (2016) Study of biomechanical, anatomical, and physiological properties of scorpion stingers for developing biomimetic materials. *Materials Science and Engineering: C* 58, 1112–1121. doi:10.1016/j.msec.2015.09.082

Data availability. The data that support this study are available as supplemental data files associated with this work at OSF (Supplemental Fig. 1: 10.17605/OSF.IO/GD7TV) and MorphoSource.org (ark:/87602/m4/495251).

Conflicts of interest. The authors declare no conflict of interest.

Declaration of funding. This research was supported by funding from an Australian Research Council Discovery Project grant (DP200102005 to JRP and GDE), UNE Postdoctoral Research Fellowships (to RDCB and CHR), and an MAT Postdoctoral Fellowship (to RDCB).

Acknowledgements. We thank Jeffrey Shultz for discussions on muscle groups and homologies, as well as four anonymous reviewers, Carolin Haug, and Paul Cooper for the constructive feedback that has improved the manuscript.

Author affiliations

^APalaeoscience Research Centre, School of Environmental & Rural Science, University of New England, Armidale, NSW 2351, Australia.

^BDivision of Paleontology (Invertebrates), American Museum of Natural History, New York, NY, 10027, USA.

^CThe Natural History Museum, London SW7 5BD, UK.

^DSchool of Ocean and Earth Science, University of Southampton Waterfront Campus, National Oceanography Centre, Southampton, SO14 3ZH, UK.

^EAustralian Museum Research Institute, Australian Museum, 1 William Street, Sydney, NSW 2010, Australia.

^FSchool of Science and Technology, University of New England, Armidale, NSW 2351, Australia.